

Theory of surface nuclear magnetic resonance with applications to geophysical imaging problems

Peter B. Weichman,¹ Eugene M. Lively,¹ and Michael H. Ritzwoller²

¹*Blackhawk Geometrics, Suite B, 301 Commercial Road, Golden, Colorado 80401*

²*Department of Physics, University of Colorado, Boulder, Colorado 80309-0390*

(Received 28 January 1999; revised manuscript received 10 February 2000)

The general theory of nuclear magnetic resonance (NMR) imaging of large electromagnetically active systems is considered. We emphasize particularly noninvasive geophysical applications such as the imaging of subsurface water content. We derive a general formula for the NMR response voltage, valid for arbitrary transmitter and receiver loop geometry and arbitrary conductivity structure of the medium in which the nuclear spins reside. It is shown that in cases where the conductivity is large enough such that the electromagnetic skin depth at the Larmor frequency is of the same order or smaller than the measurement depth, there are diffusive retardation time effects that significantly alter the standard NMR response formula used in the literature. The formula now includes the full complex response, the imaginary part of which has previously been observed but not modeled. These differences are quantified via numerical investigation of various effectively one-dimensional model inverse problems with a horizontally stratified nuclear spin and conductivity distribution. It is found that inclusion of the imaginary part of the response significantly stabilizes the inversion. Large quantitative differences are found between conducting and insulating cases in physically relevant situations. It is shown also that the diffusive long time tail of the signal may be used to infer the distribution of time constants T_1 , normally not measurable in geophysical applications. Although in present applications the signal due to this tail is immeasurably small, this relationship may become useful in the future.

PACS number(s): 41.20.-q, 47.55.Mh, 76.60.Pc, 93.85.+q

I. INTRODUCTION

The nuclear magnetic resonance (NMR) technique [1] allows one to obtain information about the nuclear spin equilibrium thermodynamics and nonequilibrium dynamics in an atomic, molecular, or condensed matter system. The measured NMR voltage is a superposition of ac signals arising from all the precessing nuclear spins within the field of view, and the Larmor frequency and decay rates of the signal may be used to obtain information about the physical and chemical environments of the spins. By varying in a controlled manner the geometry of the applied dc and ac fields, a spatial image of the nuclear spin density may be obtained from an appropriate inversion of the data, and this is the basis, for example, of medical magnetic resonance imaging (MRI).

This paper is concerned mainly with noninvasive geophysical applications of *surface* NMR [2], in which both transmitter and receiver loops are restricted to the Earth's surface [3]. The depth to which an NMR tipping pulse may be transmitted from the Earth's surface, and the return signal subsequently detected, is fundamentally limited by the Larmor frequency of the nuclear spins. The earth has a significant conductivity (varying roughly in the range 0.02–1 S/m depending mainly on salinity). The electromagnetic (EM) skin depth then falls below 1 m at frequencies in the range 0.25–10 MHz, and below 100 m at frequencies in the range 25–1000 Hz.

The Larmor frequency of an otherwise unperturbed proton (hydrogen nucleus) spin in the Earth's magnetic field, $B_e \approx 0.5G$, is $\nu_L \approx 2.1$ kHz. Since atomic scale internal fields are always much larger than B_e , this limits the detectable substances to those with effectively vanishing internal fields. Hydrogen containing compounds, such as water and hydrocarbons in the liquid state, are the primary examples of such

substances. The rapid motion of the molecules in the liquid state effectively averages the atomic scale fields to zero (an effect known as "motional narrowing"). Detectable quantities of liquid hydrocarbons rarely lie within 100 m of the Earth's surface, so the main application of geophysical surface NMR tools is to the imaging of subsurface water [4–6].

The object of this paper is to provide a rigorous theoretical basis for the geophysical water imaging problem, and for specificity most of our physical estimates will be based upon this application. The theory we develop, however, is completely general and applicable to any surface NMR imaging problem, even though the physical frequency and length scales may vary considerably (the example of high-field medical MRI is discussed briefly below). To obtain maximal depth sensitivity it is crucial to account properly for the non-trivial EM properties of the Earth [7]. In addition to the obvious exponential decay of the amplitude of the rf signal on the scale of the skin depth, we will show that there is an even more important *phase delay* effect arising from the slow, diffusive nature of EM propagation in a conducting medium. This effect will be shown to be important even at depths considerably less than the skin depth. Although special cases have been recognized in the literature [8], this phase delay effect has never, to our knowledge, been considered in the full generality necessary for quantitative spatial image reconstruction.

These same effects occur in high field medical MRI. Estimates based on frequency dependent permittivity and conductivity data for human tissues [9] show that typical skin depths fall below 10 cm and typical wavelengths fall below 30 cm as the applied field rises above about 2 T [10]. One may then expect the conductivity effects we discuss to become extremely important as the applied field is pushed into the multi-Tesla range (8 T full body systems now exist). In particular, the applied ac field may be expected to vary

substantially in amplitude through the body. However, medical imaging is concerned mainly with resolving sharp boundaries between different types of tissue (bone surfaces, blood vessel walls, etc.). Since positional resolution is determined by uniformity of applied gradients in the dc field (which are degraded by variations in magnetic permeability rather than conductivity [11]), it turns out that as long as the ac field variation is reasonably smooth over the imaged region, excellent images of such qualitative variations in the tissue properties may still be obtained [12].

In contrast, *quantitative* measurements, say, of proton spin density in a given region (as is of primary importance in geophysical applications) requires accurate modeling of the ac field amplitude and phase variations and full attention to the imaging theory developed in this paper. Due to the complex structure of the human body, such modeling is very difficult [13]. Exploring these issues in detail is important work for the future, but lies beyond the scope of the present paper.

The outline of the rest of this paper is as follows. In Sec. II we use the Maxwell equations in a conducting medium, together with the specified geometry of the NMR transmitter and receiver loops, to derive a general *imaging equation*, which takes the form of an integration kernel that produces the measured NMR voltage when integrated against a given subsurface water distribution. It is shown that this kernel reduces to the standard one used in the literature [4–6] only in a certain “adiabatic” limit in which the nuclear spin dynamics is slow compared to all environmental diffusive relaxation times, for example, for an insulating Earth.

In Sec. III we consider some simple examples. The phase delay effect is illustrated quantitatively for the simplest analytically treatable case of a point dipole in an infinite homogeneous conducting medium. The fields in the presence of a homogeneous conducting half-space are also introduced for later numerical computations.

In Sec. IV we carefully pose the inverse problem in which a series of NMR voltage measurements is used to infer the water distribution, and in Sec. V we study this problem numerically. Large deviations from the adiabatic (insulating) limit are observed in physical parameter ranges commonly characteristic of geophysical field measurements. The inclusion of the imaginary part of the imaging data is shown to add an independent datum to the inversion process, thereby improving the resolution of the estimated model. We show also that in a conducting earth the NMR signal has a late time dc tail whose amplitude is determined by the distribution of T_1 decay times. Unfortunately, in present applications the level of this signal is immeasurably low. Future experiments may, however, be capable of making use of this relationship.

II. FUNDAMENTAL EQUATION GOVERNING NMR RESPONSE

A. Nuclear magnetization dynamics

In the absence of the applied ac field, the applied static field \mathbf{B}_0 polarizes the nuclear spins according to [1]

$$\mathbf{M}_N^{(0)}(\mathbf{r}) = 1.70 \times 10^{-10} M_N^{\text{sat}} \frac{B_0}{B_e} \frac{n_N(\mathbf{r})}{2n_{\text{H}_2\text{O}}} \frac{T_{\text{room}}}{T} \hat{\mathbf{B}}_0, \quad (2.1)$$

where $B_e = 0.5 \text{ G}$, $M_N^{\text{sat}} = 2n_{\text{H}_2\text{O}}\mu_N = 0.94 \text{ erg/G cm}^3$ is the saturated magnetization that would be observed in bulk water if all the nuclear moments were aligned, $n_N(\mathbf{r})$ is the number density of nuclear magnetic moments at position \mathbf{r} (equal to twice the number density of water), $n_{\text{H}_2\text{O}} = 3.35 \times 10^{22} \text{ cm}^{-3}$ is the bulk molecular number density of water, $T_{\text{room}} = 300 \text{ K}$, and $\hat{\mathbf{B}}_0$ is a unit vector along the static field. The ratio $n_N/2n_{\text{H}_2\text{O}}$ is just the porosity of the medium. This formula indicates that a net imbalance of barely one in ten billion of the nuclear moments, corresponding to roughly six moments in each cubic micron of volume, align with the Earth’s field. However, in a volume 100 m on a side a net imbalance of about 10 moles of spins (equivalent to 90 cm³ of saturated water) are aligned, and therein lies the feasibility of the technique.

The ac field $\mathbf{B}_T(\mathbf{r}, t)$ generated by the transmitter coil causes \mathbf{M}_N to tip away from, and subsequently precess about, \mathbf{B}_0 at the (angular) Larmor frequency $\omega_L = 2\pi\nu_L = \gamma B_0$. Here $\gamma = 26,752 \text{ G}^{-1} \text{ s}^{-1}$ for the proton, is the gyromagnetic ratio. Explicitly, let $\mathbf{B}_T^\perp = \mathbf{B}_T - (\hat{\mathbf{B}}_0 \cdot \mathbf{B}_T)\hat{\mathbf{B}}_0$ be the component of \mathbf{B}_T perpendicular to \mathbf{B}_0 , and let $\mathbf{B}_T^\pm = \mathbf{B}_T^\perp \pm \mathbf{B}_T^\perp$ be the decomposition of this orthogonal field into circularly polarized co-rotating and counter-rotating components (see Sec. IV for the mathematical procedure for accomplishing this decomposition). The co-rotating component \mathbf{B}_T^+ rotates clockwise around \mathbf{B}_0 at the Larmor frequency, and the magnetization evolves according to [1]

$$\begin{aligned} \mathbf{M}_N(\mathbf{r}, t) = & \mathbf{M}_N^{(0)}(\mathbf{r}) \cos[\theta_T(\mathbf{r}, t)] + [\mathbf{M}_N^{(0)}(\mathbf{r}) \times \hat{\mathbf{B}}_T^+(\mathbf{r}, t)] \\ & \times \sin[\theta_T(\mathbf{r}, t)], \end{aligned} \quad (2.2)$$

where $\mathbf{M}_N^{(0)} = \chi_N \mathbf{B}_0$ is the equilibrium nuclear magnetization density due to the Earth’s field, $\hat{\mathbf{B}}_T^+(\mathbf{r}, t)$ is a unit vector pointing along $\mathbf{B}_T^+(\mathbf{r}, t)$, and the tipping angle is given by $\theta_T(\mathbf{r}, t) = \omega_T(\mathbf{r})t$, in which t is being measured from the onset of the transmitter field, and the tipping rate $\omega_T(\mathbf{r}) \equiv \gamma|\mathbf{B}_T^+(\mathbf{r})|$ is time independent if the magnitude of \mathbf{B}_T^+ is time independent. Thus \mathbf{M}_N lags \mathbf{B}_T^+ by 90°, and the angle of the precessing spin increases at constant rate ω_T . Equation (2.2) is obtained by transforming the usual rotating frame expression back into the laboratory frame, and is required in this form for the computations that follow. The magnetization generates an associated nuclear magnetic current [14]

$$\mathbf{j}_N = c \nabla \times \mathbf{M}_N \quad (2.3)$$

which then serves as a source term in the Maxwell equations for the corresponding nuclear magnetic field $\mathbf{B}_N(\mathbf{r}, t)$ (see below).

Note that even for an insulating earth the transmitted field decays rapidly far from the transmitter loop, and, as a rule of thumb, spins will not be tipped substantially at distances larger than the diameter of this loop. In typical applications, 100-m-diam circular or figure-eight loops are used. Currents in the range 200–300 A are generated, which then yield fields in the 10⁻² G range roughly within the (100 m)³ volume below the loop. Thus $\omega_T/\omega_L \sim 0.02$ and hence $\nu_T \equiv \omega_T/2\pi \sim 40 \text{ Hz}$.

After the transmitter field is shut off after a pulse time τ_p , the magnetization will continue to precess for some time at the fixed angle $\theta_T(\mathbf{r}, \tau_p)$. However, various decay processes act continuously and lead to an exponential decay of the magnetization back to its equilibrium form. This involves both an increase in the component along the Earth's field and a decrease in the components orthogonal to it. The decay processes in general act differently on these two components, and a phenomenological form for \mathbf{M}_N is

$$\begin{aligned} \mathbf{M}_N(\mathbf{r}, t) = & \mathbf{M}_N^{(0)}(\mathbf{r}) \{1 - e^{-(t-\tau_p)/T_1(\mathbf{r})} + e^{-(t-\tau_p)/T_1(\mathbf{r})} \\ & \times \cos[\theta_T(\mathbf{r}, \tau_p)]\} + e^{-(t-\tau_p)/T_2(\mathbf{r})} \\ & \times [\mathbf{M}_N^{(0)}(\mathbf{r}) \times \hat{\mathbf{B}}_T^+(\mathbf{r}, t)] \sin[\theta_T(\mathbf{r}, \tau_p)], \end{aligned} \quad (2.4)$$

where T_1 and T_2 are the longitudinal and transverse time constants, respectively [15]. Clearly, these same decay processes are acting during the time interval $0 < t < \tau_p$ as well, and the extrapolated origins τ_l and τ_t of the decay are actually given approximately by $\tau_p/2$ rather than τ_p itself. Both this $\tau_p/2$ rule and validity of (2.2) in this time interval depend implicitly on an assumption that $\tau_p \ll T_1, T_2$ is short compared to the decay times.

We comment that the transmitter current does not turn on and off instantaneously, and there will be some additional delay time τ_d between the switching of the current and the switching of the transmitted magnetic field as it propagates into the ground. During the switching of the transmitted field pulse at a point \mathbf{r} in the ground, the magnetization may undergo some complicated dynamics. However, as long as the duration τ_{sw} of the switching is small compared to the pulse length τ_p , and so long as $\omega_T \ll \omega_L$, this dynamics will tip the nuclear spins by a very small angle, of order $\omega_T \tau_{sw} \ll \omega_T \tau_p$, and will therefore correct the final precession angle $\theta(\tau_p)$, as well as the azimuthal phase of the precessing spin, by an amount of order τ_{sw}/τ_p . Thus, as long as one has the triple separation of time scales $\tau_{sw} \sim \tau_d \ll \tau_p \ll T_2$, the magnetization dynamics will be governed accurately by (2.2) and (2.4).

B. NMR voltage

The measured observable is the induced voltage, $V_R(t)$, in a receiver coil due to the time evolution of the subsurface nuclear magnetization in response to the applied field

$$V_R(t) = -\frac{1}{c} \frac{d\Phi_R}{dt}, \quad (2.5)$$

where $\Phi_R(t)$ is the time varying magnetic flux through the receiver loop

$$\Phi_R(t) = \int_{S_R} \mathbf{B}(\mathbf{r}, t) \cdot \hat{\mathbf{n}} dA = \int_{C_R} \mathbf{A}(\mathbf{r}, t) \cdot d\mathbf{l} \quad (2.6)$$

where $\mathbf{B} = \nabla \times \mathbf{A}$ is the total magnetic field from all sources, and S_R denotes a surface spanning the receiver loop C_R . In many applications the transmitter coil, which generates the applied field, is the same as the receiver coil. This actually simplifies certain calculations (see below), but we will not specialize to this case until the end.

It is convenient to express (2.6) as a volume integral using appropriate δ functions to limit the contributions to the curve C_R . Thus, let the closed curve C_R be parametrized by

$$\boldsymbol{\gamma}_R(s), \quad 0 \leq s \leq l_R, \quad \boldsymbol{\gamma}(0) = \boldsymbol{\gamma}(l_R). \quad (2.7)$$

The unit vector $\hat{\mathbf{t}}(s) = \partial_s \boldsymbol{\gamma}(s) / |\partial_s \boldsymbol{\gamma}(s)|$ is the tangent vector to the curve at s . If C_R is parametrized by path length, then $|\partial_s \boldsymbol{\gamma}_R(s)| \equiv 1$ and l_R becomes the length of the curve. In any case, define the vector field

$$\mathcal{J}_R(\mathbf{r}) = \int_0^{l_R} ds \partial_s \boldsymbol{\gamma}_R(s) \delta(\mathbf{r} - \boldsymbol{\gamma}_R(s)). \quad (2.8)$$

Clearly \mathcal{J}_R vanishes unless \mathbf{r} lies on the curve C_R . It is easy to check that this integral is independent of the parametrization of the curve C_R . Also, if $\mathcal{J}_R(\mathbf{r})$ is integrated over a small surface element cutting the curve at $\mathbf{r} = \boldsymbol{\gamma}(s_0)$, the result is the tangent vector $\hat{\mathbf{t}}(s_0)$. It follows then that (2.6) may be rewritten in the form

$$\Phi_R(t) = \int d^3r \mathbf{A}(\mathbf{r}, t) \cdot \mathcal{J}_R(\mathbf{r}). \quad (2.9)$$

Physically, $\mathcal{J}_R(\mathbf{r})$ is the current density associated with an ideal unit current flowing along the curve C_R .

C. Computation of the physical applied field

It is useful to define *two* magnetic field distributions in the *absence* of any nuclear magnetic effects. The first is the physical field resulting from currents in the transmitter coil. The second is a mathematically constructed *adjoint field*, related to the fictitious receiver coil current \mathcal{J}_R , that enters the formula for the NMR response.

We define the physical field first. Let $\mathbf{B}_T(\mathbf{r}, \omega) e^{-i\omega t}$ be the magnetic field distribution generated by an oscillating current, $I_T(t) = I_T^0 e^{-i\omega t}$ in the transmitter coil (the frequency here will, of course, ultimately become the Larmor frequency of the nuclear spins). For an ideal wire, the corresponding current density will take the form $I_T^0 \mathcal{J}_T(\mathbf{r})$, in which $\mathcal{J}_T(\mathbf{r})$ is defined by the analog of (2.8) for the transmitter loop. The computation of this field requires that the subsurface permeability, $\mu(\mathbf{r})$, and permittivity, $\epsilon(\mathbf{r}) = \epsilon'(\mathbf{r}) + 4\pi i \sigma'(\mathbf{r})/\omega$, distributions be given. Here $\epsilon'(\omega)$ and $\sigma'(\omega)$ are defined to be real and parametrize the real and imaginary parts of the dielectric function. Since the physical time-domain fields are real, both ϵ' and σ' are *even* functions of frequency. At the low frequencies of interest to geophysical applications ϵ' is the bound charge dc dielectric constant and σ' is the free charge dc conductivity. More generally, for higher frequency applications, independent measurements of $\epsilon'(\omega)$, $\sigma'(\omega)$, and $\mu(\omega)$ must be obtained for input into the present theory [9]. These quantities are generally second rank tensors, but we ignore this possibility and assume an isotropic medium here. Of primary interest will be the values of these fields in the subsurface. The corresponding vector potential $\mathbf{A}_T(\mathbf{r}, \omega)$ is defined in the usual way via $\mathbf{B}_T(\mathbf{r}, \omega) = \nabla \times \mathbf{A}_T(\mathbf{r}, \omega)$.

The Maxwell equations may be reduced to a single equation for the vector potential [14],

$$\nabla \times \left(\frac{1}{\mu} \nabla \times \mathbf{A} \right) - \epsilon k^2 \mathbf{A} = \frac{4\pi}{c} \mathbf{j}_S, \quad (2.10)$$

where $k = \omega/c$, $\epsilon = \epsilon' + 4\pi i \sigma' / \omega$ is the complex dielectric constant, and $\mathbf{j}_S(\mathbf{r})$ is the total current density from all sources. A gauge has been chosen so that the electric field is just $\mathbf{E} = ik\mathbf{A}$. It is convenient to define the operator

$$\mathcal{L}(\mu, \epsilon', \sigma'; \omega) = \nabla \times \left(\frac{1}{\mu} \nabla \times \right) - \epsilon k^2 \mathbf{I}, \quad (2.11)$$

which then allows us to express (2.10) in the compact form $\mathcal{L}\mathbf{A} = (4\pi/c)\mathbf{j}_S$. Here, \mathbf{I} is the 3×3 identity matrix. The solution \mathbf{A}_T is then to be obtained from this equation by substituting an appropriate form for \mathbf{j}_S —typically the given current I_T flowing in an ideal transmitter coil wire.

The low frequency form of Eq. (2.10) may be converted to time domain with the simple correspondence $-i\omega \rightarrow \partial_t$, yielding

$$\nabla \times \left(\frac{1}{\mu} \nabla \times \mathbf{A} \right) + \frac{1}{c^2} (\epsilon' \partial_t^2 + 4\pi \sigma' \partial_t) \mathbf{A}(\mathbf{r}, t) = \frac{4\pi}{c} \mathbf{j}_S(\mathbf{r}, t), \quad (2.12)$$

which is then a wave equation with $c^2/\epsilon' = v^2$ being the local speed of light in the subsurface, and an added linear time derivative dissipative term, which leads to a basic free decay time, $\tau_d = 4\pi\sigma'/\epsilon'$, of the fields in the absence of \mathbf{j}_S .

D. Computation of adjoint fields

The Hermitian adjoint of the operator \mathcal{L} is given by

$$\begin{aligned} \mathcal{L}^\dagger(\omega) &= \nabla \times \left(\frac{1}{\mu^*} \nabla \times \right) - \epsilon^* k^2 \mathbf{I} \\ &= \mathcal{L}(-\omega) \\ &= \mathcal{L}(\mu^*, \epsilon', -\sigma'; \omega). \end{aligned} \quad (2.13)$$

At low frequencies μ is real, and it is the presence of dissipation through a nonzero conductivity that leads to non-self-adjointness.

If $\mathbf{A}(\mathbf{r}, \omega)$ is the solution to (2.10), we define now the adjoint field $\tilde{\mathbf{A}}(\mathbf{r}, \omega)$ as the solution to

$$\mathcal{L}^\dagger(\omega) \tilde{\mathbf{A}} = \frac{4\pi}{c} \mathbf{j}_S. \quad (2.14)$$

Below we will require an adjoint field that is a solution to (2.14) in which \mathbf{j}_S is replaced by a form involving \mathcal{J}_R .

In the low frequency limit we recover (2.12), but with the substitution $\sigma' \rightarrow -\sigma'$. Solutions to (2.12) are causal [$\mathbf{A}(\mathbf{r}, t)$ is sensitive only to earlier time currents, $\mathbf{j}_S(\mathbf{r}, t')$ with $t' < t$], but solutions to the adjoint equation are anti-causal [$\tilde{\mathbf{A}}(\mathbf{r}, t)$ is sensitive only to later time currents, $\mathbf{j}_S(\mathbf{r}, t')$ with $t' > t$]. These causality properties are general, not limited to the low frequency limit [14].

E. NMR response for given applied field and nuclear magnetization

The contribution to the receiver flux from magnetic sources in the ground may now be computed as follows. From (2.9) one has

$$\begin{aligned} \Phi_R(t) &= \int \frac{d\omega}{2\pi} e^{-i\omega t} \int d^3r \mathcal{J}_R(\mathbf{r}) \cdot \mathbf{A}(\mathbf{r}, \omega) \\ &= \int \frac{d\omega}{2\pi} e^{-i\omega t} \langle \mathcal{J}_R | \mathbf{A}(\omega) \rangle, \end{aligned} \quad (2.15)$$

where the second line serves to define the usual inner product, and it should be recalled that \mathcal{J}_R is real.

Now, let $\mathcal{A}(\mathbf{r}, \omega)$ be the field associated with the fictitious current \mathcal{J}_R , and let $\tilde{\mathcal{A}}_R(\mathbf{r}, \omega)$ be the corresponding adjoint field:

$$\begin{aligned} \mathcal{L}(\omega) \mathcal{A}_R(\omega) &= \frac{4\pi}{c} \mathcal{J}_R, \\ \mathcal{L}^\dagger(\omega) \tilde{\mathcal{A}}_R(\omega) &= \frac{4\pi}{c} \mathcal{J}_R. \end{aligned} \quad (2.16)$$

Since \mathcal{J}_R is independent of ω , the relation $\mathcal{L}^\dagger(\omega) = \mathcal{L}(-\omega)$ implies that $\tilde{\mathcal{A}}_R(\omega) = \mathcal{A}_R(-\omega)$. The Fourier transform of the right-hand side of (2.16) is given by $(4\pi/c)\mathcal{J}_R(\mathbf{r})\delta(t)$, so that $\mathcal{A}_R(\mathbf{r}, t)$ is the response and $\tilde{\mathcal{A}}_R(\mathbf{r}, t) = \mathcal{A}_R(\mathbf{r}, -t)$ is the adjoint response of the vector potential to a δ -function current pulse at $t=0$. For example, the time domain form of (2.16) becomes

$$\begin{aligned} \nabla \times \left[\frac{1}{\mu} \nabla \times \tilde{\mathcal{A}}_R(\mathbf{r}, t) \right] + \frac{1}{c^2} (\epsilon' \partial_t^2 - 4\pi \sigma' \partial_t) \tilde{\mathcal{A}}_R(\mathbf{r}, t) \\ = \frac{4\pi}{c} \mathcal{J}_R(\mathbf{r}) \delta(t). \end{aligned} \quad (2.17)$$

By causality, $\mathcal{A}_R(\mathbf{r}, t)$ vanishes for $t < 0$ and $\tilde{\mathcal{A}}_R(\mathbf{r}, t)$ vanishes for $t > 0$.

From (2.10) one may derive the following identity:

$$\begin{aligned} \langle \mathcal{J}_R | \mathbf{A}(\omega) \rangle &= (c/4\pi) \langle \mathcal{L}^\dagger(\omega) \tilde{\mathcal{A}}_R(\omega) | \mathbf{A}(\omega) \rangle \\ &= (c/4\pi) \langle \tilde{\mathcal{A}}_R(\omega) | \mathcal{L}(\omega) \mathbf{A}(\omega) \rangle \\ &= \langle \tilde{\mathcal{A}}_R(\omega) | \mathbf{j}(\omega) \rangle, \end{aligned} \quad (2.18)$$

which yields

$$\begin{aligned} \Phi_R(t) &= \int d^3r \int_0^\infty dt' \tilde{\mathcal{A}}_R(\mathbf{r}, -t') \cdot \mathbf{j}(\mathbf{r}, t-t') \\ &= \int d^3r \int_0^\infty dt' \mathcal{A}_R(\mathbf{r}, t') \cdot \mathbf{j}(\mathbf{r}, t-t') \end{aligned} \quad (2.19)$$

in which $\mathbf{j} = \mathbf{j}_T + \mathbf{j}_R + \mathbf{j}_N$ is the physical current density arising from both the NMR apparatus and the nuclear spins. The contribution from \mathbf{j}_T , representing the mutual inductance between the transmitter and receiver coils (in the presence of the ground), will be extremely large while the transmitter

coil is turned on, and will in general swamp all other contributions [16]. It is for this reason that typical experimental protocols call for taking data only *after* a suitable lag time following turn off of the transmitter coil. The contribution from \mathbf{j}_R represents the self-inductance of the receiver coil in the presence of the ground, and is subject to the design of the experimental apparatus. Both these contributions may then be thought of as additive noise terms that degrade the NMR measurement. Finally, using $\mathbf{j}_N = c \nabla \times \mathbf{M}_N$, the contribution of interest from the nuclear spin dynamics may be written in the form

$$\frac{1}{c} \Phi_R^N(t) \equiv \int d^3r \int_0^\infty dt' \mathcal{B}_R(\mathbf{r}, t') \cdot \mathbf{M}_N(\mathbf{r}, t-t'), \quad (2.20)$$

in which an integration by parts has been performed and $\mathcal{B}_R(\mathbf{r}, t) = \nabla \times \mathcal{A}_R(\mathbf{r}, t)$ is the corresponding magnetic field. The measured voltage due to the nuclear spins is

$$V_R^N(t) = - \int d^3r \int_0^\infty dt' \mathcal{B}_R(\mathbf{r}, t') \cdot \partial_t \mathbf{M}_N(\mathbf{r}, t-t'). \quad (2.21)$$

This relation is the basic result of this section. In comparison with real data, it might be more convenient to Fourier analyze the voltage signal to obtain

$$V_R^N(\omega) = i\omega \int d^3r \mathcal{B}_R(\mathbf{r}, \omega) \cdot \mathbf{M}_N(\mathbf{r}, \omega). \quad (2.22)$$

Results for \mathcal{B}_R , to be described below, are most simply computed in Fourier space. The frequency spectrum of \mathbf{M}_N will generally consist of a strong peak, broadened by dephasing and equilibration effects, centered on the Larmor frequency. Thus \mathcal{B}_R actually need only be computed in a neighborhood of the Larmor frequency.

Equation (2.21) shows that the receiver signal at time t has contributions from the nuclear magnetization over a range of times $t' < t$ determined by the ‘‘memory function’’ \mathcal{B}_R . As shown above, this function represents a spreading magnetic signal due to a current pulse in the receiver loop. The contribution to the flux at time t is then determined by the interaction of the time reverse of this signal with the various nuclear spins that it encounters as it moves backward in time. Physically, of course, exactly the opposite is happening: each nuclear spin is sending out a spreading signal forward in time that eventually crosses the receiver loop at a later time. The interaction of this signal with the receiver loop geometry is then encoded in \mathcal{B}_R . These two equivalent views basically constitute the *reciprocity relation* that is exhibited mathematically in (2.18).

In nonconducting media, the memory time $\tau_d \sim L/c$ is set by the light crossing time of the measurement region with linear dimension L . This time is typically a few tenths of a microsecond and therefore is orders of magnitude smaller than the Larmor period. The dynamics of \mathbf{M}_N is therefore very slow on the scale of τ , and the adiabatic limit discussed below is relevant.

On the other hand, in conducting media $\tau_d \sim L^2/D$ will be set by the diffusion constant $D = c^2/4\pi\mu\sigma'$ [essentially the inverse of the coefficient of the linear time derivative in

(2.12)]: the δ -function current pulse will lead to a *diffusive* penetration of the fictitious magnetic field \mathcal{B}_R into the medium. As will be seen below, after the initial arrival of the signal there is also a slow power-law falloff, which then also sets the temporal width of the memory function. In mks units one may write, using scales appropriate to the geophysical problem,

$$D = \frac{1}{\pi} \left(\frac{\rho'}{1 \text{ } \Omega \text{ m}} \right) \left(\frac{100 \text{ m}}{1 \text{ ms}} \right)^2, \quad (2.23)$$

where we have taken $\mu/\mu_0 = 1$, and $\rho' = 1/\sigma'$ is the resistivity measured in ohm meters. This leads to

$$\tau_d = L^2/D = \pi \left(\frac{L}{100 \text{ m}} \right)^2 \left(\frac{1 \text{ } \Omega \text{ m}}{\rho'} \right) \text{ ms}. \quad (2.24)$$

If the dimensionless product

$$\omega_L \tau_d = 2\pi^2 \left(\frac{\nu_L}{1 \text{ kHz}} \right) \left(\frac{L}{100 \text{ m}} \right)^2 \left(\frac{1 \text{ } \Omega \text{ m}}{\rho'} \right) \quad (2.25)$$

is of order unity, the memory time will have a significant effect. For $\nu_L = \omega_L/2\pi = 2 \text{ kHz}$ and $L = 50 \text{ m}$, this will occur for resistivities lower than of order $10 \text{ } \Omega \text{ m}$. Noting that the skin depth at frequency ω is given by $\delta_s = \sqrt{2D/\omega}$ [14], one may write $\omega_L \tau_d = 2L^2/\delta_s^2$. An equivalent statement is then that the memory time will be significant if the electromagnetic skin depth at the Larmor frequency is comparable to the length scale of the measurement.

The estimates above will be confirmed explicitly for various model problems. In Sec. III complete analytic solutions for the simplest possible case, that of a point dipole in an infinite homogeneous conducting medium, are given.

As a final note, in principle one must consider the diffusion of \mathbf{B}_T into the subsurface after the tipping pulse is turned on. We ignore this in all of our calculations because we assume that the time taken to tip the spin is much larger than the Larmor period, $\omega_T/\omega_L \ll 1$. Under most conditions one should also have $\omega_T \tau_d \ll 1$ so that the tipping dynamics is affected very little by delay effects.

F. The adiabatic limit

In physical, chemical, and medical applications, the NMR measurement probes a relatively small region of space at frequencies where the EM skin depth is much larger than the sample being probed. In this case the memory time τ_d is much shorter than the Larmor period. One then has $\mathbf{M}_N(\mathbf{r}, t-t') \approx \mathbf{M}_N(\mathbf{r}, t)$ over the relevant range of t' , and the time integral in (2.20) may effectively be carried out only over \mathcal{B}_R . One obtains then

$$\frac{1}{c} \Phi_R^N(t) = \int d^3r \mathcal{B}_R^0(\mathbf{r}) \cdot \mathbf{M}_N(\mathbf{r}, t) \quad (2.26)$$

where

$$\mathcal{B}_R^0(\mathbf{r}) = \int_0^\infty dt \mathcal{B}(\mathbf{r}, t), \quad (2.27)$$

which, from (2.17), then satisfies the static equation

$$\nabla \times \left(\frac{1}{\mu} \mathbf{B}_R^0 \right) = \frac{4\pi}{c} \mathcal{J}_R. \quad (2.28)$$

The solution to this equation is precisely the Biot-Savart law for the static magnetic field generated by the static current source \mathcal{J}_R . The measured voltage in this limit is then given by

$$V_R^N(t) = - \int d^3r \mathbf{B}_R^0(\mathbf{r}) \cdot \partial_t \mathbf{M}_N(\mathbf{r}, t). \quad (2.29)$$

Now, the tipping dynamics of $\mathbf{M}_N(\mathbf{r}, t)$ is determined by the transmitter loop field $\mathbf{B}_T(\mathbf{r}, t)$, through (2.2). In the adiabatic limit in which the transmitter current varies slowly compared to any delay time, the transmitter current $I_T(t)$ and the actual transmitted field will be in phase:

$$\mathbf{B}_T(\mathbf{r}, t) = I_T(t) \mathbf{B}_T^0(\mathbf{r}), \quad (2.30)$$

where $\mathbf{B}_T^0(\mathbf{r})$ is the field due to a static unit current in the transmitter coil. In many applications, the receiver and transmitter coils are coincident. In this case $\mathbf{B}_T^0(\mathbf{r}) = \mathbf{B}_R^0(\mathbf{r})$. For NMR applications one chooses $I_T(t) = I_T^0 \cos(\omega_L t + \varphi)$, where φ is an arbitrary phase. One obtains then for the co-rotating part of the transmitter field,

$$\begin{aligned} \mathbf{B}_T^\perp(\mathbf{r}, t) = & \frac{1}{2} I_T^0 \left[\mathbf{B}_T^{0\perp}(\mathbf{r}) \cos(\omega_L t + \varphi) \right. \\ & \left. - \hat{\mathbf{B}}_0 \times \mathbf{B}_T^{0\perp}(\mathbf{r}) \sin(\omega_L t + \varphi) \right] \end{aligned} \quad (2.31)$$

where $\mathbf{B}_T^{0\perp}(\mathbf{r}) = \mathbf{B}_T^0(\mathbf{r}) - [\hat{\mathbf{B}}_0 \cdot \mathbf{B}_T^0(\mathbf{r})] \hat{\mathbf{B}}_0$ is the component of \mathbf{B}_0 orthogonal to the Earth's field. To simplify the notation, define the (static) unit vector $\hat{\mathbf{b}}_T^0(\mathbf{r}) \equiv \mathbf{B}_T^{0\perp}(\mathbf{r}) / |\mathbf{B}_T^{0\perp}(\mathbf{r})|$ in the plane perpendicular to \mathbf{B}_0 . Using (2.2) for the nuclear spin dynamics, one obtains then

$$\begin{aligned} \mathbf{M}_N(\mathbf{r}, t) = & |\mathbf{M}_N^{(0)}(\mathbf{r})| \{ \cos[\theta(\mathbf{r}, t)] \hat{\mathbf{B}}_0 \\ & + \sin[\theta(\mathbf{r}, t)] [\hat{\mathbf{B}}_0 \times \hat{\mathbf{b}}_T^0(\mathbf{r}) \cos(\omega_L t + \varphi) \\ & + \hat{\mathbf{b}}_T^0(\mathbf{r}) \sin(\omega_L t + \varphi)] \}, \end{aligned} \quad (2.32)$$

with $\theta_T(\mathbf{r}, t) = \gamma |\mathbf{B}_T^\perp(\mathbf{r})| t = \frac{1}{2} \gamma I_T^0 |\mathbf{B}_T^{0\perp}(\mathbf{r})| t$. One obtains then finally from (2.26)

$$\begin{aligned} \frac{1}{c} \Phi_R(t) = & \int d^3r |\mathbf{M}^{(0)}(\mathbf{r})| \{ \cos[\theta_T(\mathbf{r}, t)] \hat{\mathbf{B}}_0 \cdot \mathbf{B}_R^0(\mathbf{r}) \\ & + \sin[\theta_T(\mathbf{r}, t)] |\mathbf{B}_0^\perp(\mathbf{r})| [\hat{\mathbf{B}}_0 \cdot \mathbf{b}_T^0(\mathbf{r}) \times \mathbf{b}_R^0(\mathbf{r}) \\ & \times \cos(\omega_L t + \varphi) + \mathbf{b}_T^0(\mathbf{r}) \cdot \mathbf{b}_R^0(\mathbf{r}) \sin(\omega_L t + \varphi)] \}, \end{aligned} \quad (2.33)$$

where the static unit vector $\hat{\mathbf{b}}_R^0(\mathbf{r}) \equiv \mathbf{B}_R^0(\mathbf{r}) / |\mathbf{B}_R^0(\mathbf{r})|$ defined by a unit steady current the receiver loop, and also lying in the plane orthogonal to \mathbf{B}_0 , is defined analogously to $\hat{\mathbf{b}}_T^0(\mathbf{r})$.

Since the tipping rate is generally much smaller than the Larmor frequency, $\omega_T \ll \omega_L$, the dominant contribution to the voltage comes from the last two terms and yields $V_R^N(t) \equiv \bar{V}_{R,1}^N(t) \cos(\omega_L t + \varphi) + \bar{V}_{R,2}^N(t) \sin(\omega_L t + \varphi)$ with slowly varying in phase and out of phase (quadrature) envelope functions. It is mathematically convenient to combine these into the single complex number $\bar{V}_R^N(t) = \bar{V}_{R,1}^N(t) + i \bar{V}_{R,2}^N(t)$, which is then given by

$$\begin{aligned} \bar{V}_R^N(t) = & -\omega_L \int d^3r |\mathbf{B}_R^{0\perp}(\mathbf{r})| |\mathbf{M}^{(0)}(\mathbf{r})| \sin[\omega_T(\mathbf{r}) t] \\ & \times \{ \hat{\mathbf{b}}_R^0(\mathbf{r}) \cdot \hat{\mathbf{b}}_T^0(\mathbf{r}) + i \mathbf{B}_0 \cdot [\hat{\mathbf{b}}_R^0(\mathbf{r}) \times \hat{\mathbf{b}}_T^0(\mathbf{r})] \}. \end{aligned} \quad (2.34)$$

If the transmitter and receiver loops coincide, then the cross product terms vanishes in (2.33) and (2.34), and only the in-phase component survives. We will see in Sec. IV below that one of the effects of nonadiabatic corrections is to produce a quadrature component to the signal even when the two loops coincide.

If the tipping field is applied for a time τ_p , then the complex voltage envelope just after the turn-off time is

$$\begin{aligned} V(q) \equiv & \bar{V}_R^N(\tau_p^+) \\ = & - \frac{\omega_L \gamma^2 \hbar^2 S(S+1) B_0}{3 k_B T} \int d^3r |\mathbf{B}_R^{0\perp}(\mathbf{r})| n_N(\mathbf{r}) \\ & \times \sin \left[\frac{1}{2} \gamma q |\mathbf{B}_T^{0\perp}(\mathbf{r})| \right] \{ \hat{\mathbf{b}}_R^0(\mathbf{r}) \cdot \hat{\mathbf{b}}_T^0(\mathbf{r}) \\ & + i \hat{\mathbf{B}}_0 \cdot [\hat{\mathbf{b}}_R^0(\mathbf{r}) \times \hat{\mathbf{b}}_T^0(\mathbf{r})] \}. \end{aligned} \quad (2.35)$$

The pulse moment is defined as $q = I_T^0 \tau_p$, and (2.35) demonstrates explicitly that it is only this combination that enters. More generally, if the amplitude of the transmitter current varies slowly (on the scale of the Larmor period $t_L = 2\pi/\omega_L$ and the delay time τ_d), then (2.35) is still valid, but now with

$$q = \int_0^{\tau_p} I_T^0(t) dt. \quad (2.36)$$

In the case where the transmitter and receiver coils coincide, (2.35) simplifies to,

$$\begin{aligned} V(q) = & - \frac{\omega_L \gamma^2 \hbar^2 S(S+1) B_0}{3 k_B T I_T^0} \int d^3r |\mathbf{B}_{T0}^\perp(\mathbf{r})| n_N(\mathbf{r}) \\ & \times \sin \left[\frac{1}{2} \gamma \tau_p |\mathbf{B}_{T0}^\perp(\mathbf{r})| \right], \end{aligned} \quad (2.37)$$

where, in an obvious notation, we have introduced the physical total field amplitude $\mathbf{B}_{T0}(\mathbf{r}) = I_T^0 \mathbf{B}_T^0(\mathbf{r})$, whose perpendicular component appears in the equation.

If R is the radius of the loop, the characteristic field strength is $|\mathbf{B}_T^\perp| \sim 2/cR$. The expected voltage (in volts) predicted by (2.37) may be crudely estimated as $V \sim 10^{-8} c \omega_L |\mathbf{M}_N^{(0)}| |\mathbf{B}_T^\perp| R^3$, where $10^{-8} c \approx 300$ V/stat V is the voltage conversion factor from Gaussian to mks units [14]. Using $R = 50$ m, $\omega_L = 1.33 \times 10^4$ s $^{-1}$, and (2.1), one finds V

$\sim 1 \mu\text{V}$ at room temperature for bulk water. The porosity of the rock reduces typical experimental signals to the observed 100 nV range.

The relation (2.37) has been applied by a number of authors to the surface NMR problem [17]. We see now that (2.29) and (2.34) are correct only if dynamic effects, such as dissipation and retardation, are unimportant. Thus if the conductivity structure of the subsurface significantly alters the applied field, as quantified by (2.24), then (2.8) is inappropriate and (2.21) must be used in its place. A full discussion of the problem in this case will be deferred until Sec. IV below.

III. SOME SIMPLE EXAMPLES

A. Localized moment in a uniform conducting medium

To gain some insight into the fundamental result (2.21) we consider first the case of a localized current pulse $\mathbf{j}(\mathbf{r})\delta(t)$ embedded in a uniform conducting medium. This medium is taken to have $\mu=1$, and uniform conductivity $\sigma'=\sigma_0$. We assume that the frequency is low enough that ϵ' has negligible effect, and so take simply $\epsilon'=0$. From (2.12) we obtain then the basic equation

$$(\partial_t - D\nabla^2)\mathbf{A}(\mathbf{r}, t) = \frac{4\pi D}{c}\mathbf{j}(\mathbf{r})\delta(t), \quad (3.1)$$

with diffusion coefficient $D=c^2/4\pi\sigma_0$. We define the diffusion operator Green function $G(\mathbf{r}, t)$ via

$$(\partial_t - D\nabla^2)G = \delta(\mathbf{r})\delta(t). \quad (3.2)$$

The Fourier transform of this equation is simply $(-i\omega + Dq^2)G(\mathbf{q}, \omega) = 1$, where \mathbf{q} is the wave vector, with solution $G(\mathbf{q}, \omega) = (-i\omega + Dq^2)^{-1}$. Inverting the Fourier transform one obtains the frequency domain and time domain forms

$$G(\mathbf{r}, \omega) = \frac{e^{-[1-i\text{sgn}(\omega)]r/\delta_s(\omega)}}{4\pi D r}, \quad G(\mathbf{q}, t) = e^{-Dq^2 t}\theta(t), \quad (3.3)$$

$$G(\mathbf{r}, t) = \frac{e^{-r^2/4Dt}}{(4\pi Dt)^{3/2}}\theta(t),$$

where $\theta(s)$ is the unit step function, vanishing for $s < 0$, and in the first relation we have introduced the electromagnetic skin depth $\delta_s(\omega) = \sqrt{2D/|\omega|}$, which decreases as frequency and/or conductivity increase. We see explicitly the causal nature of G in the time domain. The functional coefficient of $\theta(t)$ is the standard diffusion kernel. The general solution to (3.1) is now,

$$\begin{aligned} \mathbf{A}(\mathbf{r}, t) &= \frac{4\pi D}{c} \int d^3 r' G(\mathbf{r} - \mathbf{r}', t - t') \mathbf{j}(\mathbf{r}') \delta(t') \\ &= \frac{\theta(t)}{\sqrt{4\pi D c^2 t^3}} \int d^3 r' \mathbf{j}(\mathbf{r}') e^{-|\mathbf{r} - \mathbf{r}'|^2/4Dt}. \end{aligned} \quad (3.4)$$

This demonstrates the diffusive spreading of the $t=0$ impulse [18]. The magnetic field is obtained as the curl of (3.4).

As a more specific application of (3.4), suppose that $\mathbf{j}(\mathbf{r})$ arises from an ideal magnetic moment $\mathbf{M}(\mathbf{r}) = \mathbf{m}_0 \delta(\mathbf{r})$ at the origin. From the relation $\mathbf{j} = c\nabla \times \mathbf{M}$ one obtains

$$\begin{aligned} \mathbf{A}(\mathbf{r}, t) &= \theta(t) \frac{1}{\sqrt{4\pi D t^3}} \mathbf{m}_0 \times \nabla (e^{-r^2/4Dt}) \\ &= -\theta(t) \frac{\pi}{\sqrt{2}t} \frac{e^{-r^2/4Dt}}{(4\pi D t)^{3/2}} \mathbf{m}_0 \times \mathbf{r}, \end{aligned} \quad (3.5)$$

which points in the azimuthal direction relative to the axis defined by \mathbf{m}_0 . The magnetic field takes the form

$$\begin{aligned} \mathbf{B}(\mathbf{r}, t) &= \theta(t) \frac{1}{\sqrt{4\pi D t^3}} \mathbf{m}_0 \cdot (\mathbf{I}\nabla^2 - \nabla\nabla)(e^{-r^2/4Dt}) \\ &= \theta(t) \frac{1}{t} \frac{e^{-r^2/4Dt}}{(4\pi D t)^{3/2}} \left\{ \frac{r^2}{4Dt} [\mathbf{m}_0 - (\mathbf{m}_0 \cdot \hat{\mathbf{r}})\hat{\mathbf{r}}] - \mathbf{m}_0 \right\}. \end{aligned} \quad (3.6)$$

This form shows the diffusive spreading with time of a distorted dipole field. The diffusing front arrives at position \mathbf{r} at $t \sim r^2/4D$. At large times $\mathbf{B}(\mathbf{r}, t)$ points opposite to \mathbf{m}_0 and decays with a $t^{-5/2}$ power law. As alluded to above Eq. (2.23), this power law sets the temporal width of the memory function \mathcal{B}_R . For completeness, the corresponding frequency domain forms of (3.5) and (3.6) may be evaluated as

$$\begin{aligned} \mathbf{A}(\mathbf{r}, \omega) &= \mathbf{m}_0 \times \nabla \left[\frac{1}{r} e^{-[1-i\text{sgn}(\omega)]r/\delta_s(\omega)} \right] \\ &= -e^{-[1-i\text{sgn}(\omega)]r/\delta_s(\omega)} \\ &\quad \times \left[1 + [1-i\text{sgn}(\omega)] \frac{r}{\delta_s(\omega)} \right] \frac{\mathbf{m}_0 \times \hat{\mathbf{r}}}{r^2}, \end{aligned}$$

$$\begin{aligned} \mathbf{B}(\mathbf{r}, \omega) &= \mathbf{m}_0 \cdot (\mathbf{I}\nabla^2 - \nabla\nabla) \left[\frac{1}{r} e^{-[1-i\text{sgn}(\omega)]r/\delta_s(\omega)} \right] \\ &= e^{-[1-i\text{sgn}(\omega)]r/\delta_s(\omega)} \left\{ 2i \frac{\mathbf{m}_0 - (\mathbf{m}_0 \cdot \hat{\mathbf{r}})\hat{\mathbf{r}}}{\delta_s(\omega)^2 r} \right. \\ &\quad \left. - \left[1 + [1-i\text{sgn}(\omega)] \frac{r}{\delta_s(\omega)} \right] \frac{3(\mathbf{m}_0 \cdot \hat{\mathbf{r}})\hat{\mathbf{r}} - \mathbf{m}_0}{r^3} \right\}. \end{aligned} \quad (3.7)$$

The adiabatic limit may be computed either as the zero frequency limit of (3.7), or by solving the Poisson equation, $\nabla^2 \mathbf{A}_0(\mathbf{r}) = (4\pi/c)\mathbf{j}(\mathbf{r})$, that results when (3.1) is integrated over time. Here $\mathbf{A}_0(\mathbf{r}) = \int_{-\infty}^{\infty} dt \mathbf{A}(\mathbf{r}, t)$ is the time integral of the vector potential. The Green function is now just the usual Coulomb potential, and one obtains

$$\mathbf{A}_0(\mathbf{r}) = -\frac{1}{c} \int d^3r' \frac{\mathbf{j}(\mathbf{r}')}{|\mathbf{r}-\mathbf{r}'|}. \quad (3.8)$$

For the special case of a point dipole \mathbf{m}_0 one obtains the standard dipole field [14],

$$\mathbf{B}_0(\mathbf{r}) = -\frac{3(\mathbf{m}_0 \cdot \hat{\mathbf{r}})\hat{\mathbf{r}} - \hat{\mathbf{m}}_0}{r^3} \quad (3.9)$$

which also results as the zero frequency ($\delta_s \rightarrow \infty$) limit of (3.7).

Since the NMR measurement takes place at a well defined frequency ω_L , Eq. (3.7) provides the most direct quantitative measure of diffusive effects. As discussed on general grounds below Eq. (2.25), one sees explicitly the role of the skin depth $\delta_s(\omega_L)$ in altering the form of the field from its adiabatic form, leading to the exponential decay and growth of an imaginary part of the dipole field and for distances $r > \delta_s(\omega_L)$.

B. Horizontal loop sitting on a homogeneous half-space

In later numerical computations we shall consider the case of coincident horizontal circular transmitter and receiver loops of radius r_0 lying on a homogeneous nonpermeable, conducting half-space. In future work [19] we will consider more general horizontally stratified Earth models. Defining the loop magnetic moment $m_0 = \mu \pi r_0^2 I_0 / c$, the electric fields are purely azimuthal, $\mathbf{E} = E_\phi \hat{\boldsymbol{\phi}}$, and given by [20]

$$\begin{aligned} E_\phi(r, z, \omega) &= ikA_\phi(r, k, \omega) \\ &= \frac{4ikm_0}{r_0} \int_0^\infty \frac{\lambda d\lambda}{\lambda + \tilde{\lambda}} J_1(\lambda r) J_1(\lambda r_0) \\ &\quad \times [e^{-\lambda z} \theta(z) + e^{\tilde{\lambda} z} \theta(-z)], \end{aligned} \quad (3.10)$$

where $\tilde{\lambda} = \sqrt{\lambda^2 - i\omega/D}$ with $D = c^2/4\pi\sigma'$ the subsurface diffusion constant. The radial and azimuthal components of the magnetic field are then given by

$$\begin{aligned} B_r(r, z, \omega) &= -\frac{\partial A_\phi}{\partial z} \\ &= \frac{4m_0}{r_0} \int_0^\infty \frac{\lambda d\lambda}{\lambda + \tilde{\lambda}} J_1(\lambda r) J_1(\lambda r_0) \\ &\quad \times [\lambda e^{-\lambda z} \theta(z) - \tilde{\lambda} e^{\tilde{\lambda} z} \theta(-z)], \\ B_z(r, z, \omega) &= \frac{1}{r} \frac{r \partial A_\phi}{\partial r} \\ &= \frac{4m_0}{r_0} \int_0^\infty \frac{\lambda^2 d\lambda}{\lambda + \tilde{\lambda}} J_0(\lambda r) J_1(\lambda r_0) \\ &\quad \times [e^{-\lambda z} \theta(z) + e^{\tilde{\lambda} z} \theta(-z)]. \end{aligned} \quad (3.11)$$

The λ integrations in each case must be performed numerically. For the purposes of computing the NMR response, only the Larmor frequency component of the time domain

field is required. Thus we may simply set $\omega = \omega_L$ in (3.11). Notice that a figure-eight loop may be modeled by two oppositely oriented loops displaced from each other by one loop radius, and the associated fields are therefore simple vector superpositions of the two displaced fields.

C. Scaling of the signal amplitude

From the basic results (2.21) and (2.29) for the measured voltage, one sees that the response is governed by the size of the volume over which the product $\mathcal{B}_0(\mathbf{r}) \cdot \mathbf{M}_N(\mathbf{r})$ is significant, and the overall magnitude of $\mathcal{B}_0(\mathbf{r})$ in this region. The region over which $\mathcal{B}_0(\mathbf{r})$ itself is significant scales as l^3 , the cube of the loop size. Since \mathcal{B}_0 is the response to a unit current in the loop, its overall magnitude will scale inversely with the loop size as $1/l$ in this same region. The main contribution to the voltage will come from the region over which $\mathbf{M}_N(\mathbf{r})$ has been tipped somewhere close to $\pi/2$. The surface on which the tip angle takes any particular value clearly scales as l^2 . However, the family of surfaces over which the tip angle lies in some fixed interval (say of width ϵ) about $\pi/2$ scales inversely with the *gradient* of $\mathcal{B}_0(\mathbf{r})$ [the more uniform is $\mathcal{B}_0(\mathbf{r})$, the larger the extent of the region over which the tip angle will be within the tolerance ϵ of $\pi/2$]. The local uniformity of $\mathcal{B}_0(\mathbf{r})$ scales as $1/l$, and the volume over which the dot product $\mathcal{B}_0(\mathbf{r}) \cdot \mathbf{M}_N(\mathbf{r})$ is significant will therefore scale as ϵl^3 . One concludes then that the voltage response will scale as ϵl^2 , increasing as the square of the loop size. Therefore not only does one's depth sensitivity increase with l , but one's sensitivity at a given depth generally increases as well.

If one fixes the overall length l of the wire, but lays it out in a smaller loop with multiple (say n) windings, the magnitude of $\mathcal{B}_0(\mathbf{r})$ will scale with n while the loop size scales as $1/n$. The above estimate then shows that the measured voltage will decrease as $1/n^2$: there is therefore no direct gain from multiple windings. On the other hand, one may ask a slightly different question: although overall voltage response increases with loop size, spatial resolution near a given depth (say, 20 m below the surface) scales linearly with the local magnetic field *gradient*. Since the gradient decreases as l increases, there will be a trade-off curve between overall signal-to-noise and resolving power at a given depth. Any given criterion for choosing where on this trade-off curve one would like to sit will then determine an optimum loop size. If, for a given depth, this optimum size is significantly smaller than the length of wire available, multiple windings will now provide an advantage. Determination of this trade-off curve is not a simple issue and lies at the heart of the inverse problem that will be discussed in Sec. V.

In any measurement there will be noise sources that will add additional constraints on the experimental design. The limitations of intrinsic thermal noise, which may be mitigated by averaging over many measurements, is discussed in Ref. [21]. In geophysical measurements, cultural (e.g., power lines and automobile engines) and environmental (e.g., lightning storms) noise provide the most severe limitations [22]. The former presently forbids use of the surface NMR technique in urban areas.

IV. THE INVERSE PROBLEM AND COMPUTATION OF WATER CONTENT DISTRIBUTION

A. The forward problem

The present surface NMR technique consists of measuring the voltage response, $V_R^N(t)$, of the subsurface over some time interval after application of various pulse moments $q = I_T^0 \tau_p$, where I_T^0 is the amplitude of the transmitter current, $I_T = I_T^0 \cos(\omega_L t + \varphi)$ and τ_p is the length of the pulse. This response is extrapolated back to infer the voltage $V_R^N(\tau_i)$, where $\tau_i \approx \tau_p/2$ was defined in (2.4). With the time delay effects discussed in Sec. II B 4, one should actually extrapolate back to a time several delay times τ_d after τ_i , but for $\tau_d, \tau_p \ll T_1, T_2$ these distinctions are unimportant. We begin this section by generalizing the adiabatic formula (2.36) to include delay effects.

1. Computation of the corotating field

First note that although the transmitted field oscillates at the Larmor frequency throughout the subsurface (following a build-up time of order the delay time τ_d), (2.30) must now be generalized to allow for a depth-dependent phase change:

$$\begin{aligned} \mathbf{B}_T(\mathbf{r}, t) &= I_T^0 [\mathbf{B}_{T,1}(\mathbf{r}, \omega_L) \cos(\omega_L t + \varphi) \\ &\quad + \mathbf{B}_{T,2}(\mathbf{r}, \omega_L) \sin(\omega_L t + \varphi)] \\ &= \frac{1}{2} I_T^0 [\mathbf{B}_T(\mathbf{r}, \omega_L) e^{-i(\omega_L t + \varphi)} + \mathbf{B}_T(\mathbf{r}, -\omega_L) e^{i(\omega_L t + \varphi)}] \end{aligned} \quad (4.1)$$

in which $\mathbf{B}_T(\mathbf{r}, \pm \omega_L) = \mathbf{B}_{T,1}(\mathbf{r}, \omega_L) \pm i \mathbf{B}_{T,2}(\mathbf{r}, \omega_L) = \mathbf{B}_T^*(\mathbf{r}, \mp \omega_L)$ is the complex field amplitude due to a unit complex current $I_T(t) = e^{-i(\omega_L t + \varphi)}$. The combination $I_T^0 \mathbf{B}_T(\mathbf{r}, \omega)$ is precisely the frequency domain field that is computed in Sec. III. In the adiabatic limit $\mathbf{B}_T(\mathbf{r}, \pm \omega_L) \rightarrow \mathbf{B}_T^0(\mathbf{r})$ is real and (2.30) results. Now, in a dissipative medium $\mathbf{B}_{T,1}$ and $\mathbf{B}_{T,2}$ will in general be noncollinear, corresponding to an elliptically polarized transmitted field. This can be easily checked for the example treated in Sec. II C: from (2.32), components of the magnetic field along $\mathbf{m}_0 - (\mathbf{m}_0 \cdot \hat{\mathbf{r}}) \hat{\mathbf{r}}$ and along $\mathbf{m}_0 - 3(\mathbf{m}_0 \cdot \hat{\mathbf{r}}) \hat{\mathbf{r}}$ in general have different complex weights and hence lead to noncollinear real and imaginary parts of the magnetic field. More generally, (2.10) yields very different equations for the real and imaginary parts of \mathbf{A} whenever ϵ is complex, i.e., whenever $\sigma \neq 0$. The corotating and counterrotating parts of the field then have different amplitudes. To compute the co-rotating part we decompose the components of $\mathbf{B}_T(\mathbf{r}, \omega_L)$ orthogonal to the static field \mathbf{B}_0 in the form,

$$\begin{aligned} \mathbf{B}_T^\perp(\mathbf{r}, \omega_L) &= e^{i\zeta_T(\mathbf{r}, \omega_L)} [\alpha_T(\mathbf{r}, \omega_L) \hat{\mathbf{b}}_T(\mathbf{r}, \omega_L) \\ &\quad + i\beta_T(\mathbf{r}, \omega_L) \hat{\mathbf{B}}_0 \times \hat{\mathbf{b}}_T(\mathbf{r}, \omega_L)] \end{aligned} \quad (4.2)$$

in which the phase ζ_T is chosen in such a way that α_T and β_T are real. The (static) unit vector $\hat{\mathbf{b}}_T(\mathbf{r}, \omega_L)$, lying in the plane orthogonal to \mathbf{B}_0 , generalizes the adiabatic unit vector $\hat{\mathbf{b}}_T^0(\mathbf{r})$ defined above (2.32) (and reduces to it in the limit $\omega_L \rightarrow 0$). Since $\mathbf{B}_T^\perp(\mathbf{r}, -\omega_L) = \mathbf{B}_T^{\perp*}(\mathbf{r}, \omega_L)$ it follows that $\zeta_T(\omega_L) = -\zeta_T(-\omega_L)$ and $\beta_T(\omega_L) = -\beta_T(-\omega_L)$ are odd functions

of frequency while $\alpha_T(\omega_L) = \alpha_T(-\omega_L)$ and $\hat{\mathbf{b}}_T(\omega_L) = \hat{\mathbf{b}}_T(-\omega_L)$ are even functions of frequency. By rotating $\hat{\mathbf{b}}_T^{(0)}$ by a multiple of $\pi/2$, and making a corresponding multiple of $\pi/2$ adjustment in the phase ζ_T , we may choose $\alpha_T \geq |\beta_T| \geq 0$ to be positive and $-\pi/2 < \zeta_T \leq \pi/2$. Consider then the combinations,

$$\begin{aligned} \mathbf{B}_T^\perp \cdot \mathbf{B}_T^\perp &= [\alpha_T^2 - \beta_T^2] e^{2i\zeta_T}, \\ \mathbf{B}_T^\perp \cdot \mathbf{B}_T^{\perp*} &= \alpha_T^2 + \beta_T^2, \\ \mathbf{B}_T^\perp \times \mathbf{B}_T^{\perp*} &= -2i\alpha_T\beta_T \hat{\mathbf{B}}_0. \end{aligned} \quad (4.3)$$

One obtains then

$$e^{i\zeta_T} = \sqrt{\frac{(\mathbf{B}_T^\perp)^2}{|\mathbf{B}_T^\perp|^2}} \quad (4.4)$$

in which the sign of the square root is determined uniquely by the above restriction on the range of ζ_T . The last equation determines the sign of β_T , and together with the second and the magnitude of the first, one then obtains

$$\begin{aligned} \alpha_T &= \frac{1}{\sqrt{2}} \sqrt{|\mathbf{B}_T^\perp|^2 + |(\mathbf{B}_T^\perp)^2|}, \\ \beta_T &= \text{sgn}[i\hat{\mathbf{B}}_0 \cdot \mathbf{B}_T^\perp \times \mathbf{B}_T^{\perp*}] \frac{1}{\sqrt{2}} \sqrt{|\mathbf{B}_T^\perp|^2 - |(\mathbf{B}_T^\perp)^2|}. \end{aligned} \quad (4.5)$$

The unit vector $\hat{\mathbf{b}}_T$ is now finally determined simply as

$$\hat{\mathbf{b}}_T = \frac{1}{\alpha_T} \text{Re}(e^{-i\zeta_T} \mathbf{B}_T^\perp). \quad (4.6)$$

With this decomposition we now see that the total field may be written in the form,

$$\begin{aligned} \mathbf{B}_T^\perp &= I_T^0 [\alpha_T \cos(\omega_L t + \varphi - \zeta_T) \hat{\mathbf{b}}_T \\ &\quad + \beta_T \sin(\omega_L t + \varphi - \zeta_T) \hat{\mathbf{B}}_0 \times \hat{\mathbf{b}}_T] \\ &= \mathbf{B}_T^+(\mathbf{r}, t) + \mathbf{B}_T^-(\mathbf{r}, t), \\ \mathbf{B}_T^\pm &\equiv \frac{1}{2} I_T^0 (\alpha_T \mp \beta_T) [\cos(\omega_L t + \varphi - \zeta_T) \hat{\mathbf{b}}_T \\ &\quad \mp \sin(\omega_L t + \varphi - \zeta_T) \hat{\mathbf{B}}_0 \times \hat{\mathbf{b}}_T]. \end{aligned} \quad (4.7)$$

These corotating and counterrotating components may also be expressed in the form

$$\begin{aligned} \mathbf{B}_T^\pm(\mathbf{r}, t) &= \frac{1}{2} I_T^0 [\mathbf{B}_T^\pm(\mathbf{r}, \omega_L) e^{-i(\omega_L t + \varphi)} \\ &\quad + \mathbf{B}_T^{\pm*}(\mathbf{r}, \omega_L) e^{i(\omega_L t + \varphi)}], \end{aligned} \quad (4.8)$$

in which

$$\begin{aligned}
\mathcal{B}_T^\pm(\mathbf{r}, \omega_L) &= \mathcal{B}_T^{\mp*}(\mathbf{r}, -\omega_L) \\
&= \frac{1}{2} [\alpha_T(\mathbf{r}, \omega_L) \mp \beta_T(\mathbf{r}, \omega_L)] e^{i\zeta_T(\mathbf{r}, \omega_L)} \\
&\quad \times [\hat{\mathbf{b}}_T(\mathbf{r}, \omega_L) \mp i\hat{\mathbf{B}}_0 \times \hat{\mathbf{b}}_T(\mathbf{r}, \omega_L)]. \quad (4.9)
\end{aligned}$$

The phase ζ_T now has the physical interpretation of the change in phase of the rotating field relative to that of the transmitter current. The relative phase of the precessing nuclear spins will therefore change, through (2.2), with depth as well.

As an illustration of these formal results, consider the analytic example discussed in Sec. IID. Suppose that $\mathbf{m}_0 = m_0 \hat{\mathbf{z}}$ and $\mathbf{B}_0 = B_0 \hat{\mathbf{z}}$ both point vertically. From (3.7), the field orthogonal to \mathbf{B}_0 is given by

$$\begin{aligned}
\mathbf{B}^\perp(\mathbf{r}, \omega_L) &= -\frac{3m_0 \sin(2\theta)}{2r^3} \left[1 - 2i \operatorname{sgn}(\omega) \frac{r^2}{\delta_s(\omega_L)^2} \right] \\
&\quad \times e^{-[1 - i \operatorname{sgn}(\omega)]r/\delta_s(\omega_L)} \hat{\boldsymbol{\rho}}, \quad (4.10)
\end{aligned}$$

where $\hat{\boldsymbol{\rho}}$ is the radial unit vector in the xy plane, and θ is the usual polar angle. The real and imaginary parts are collinear in this case, and the perpendicular field is therefore linearly polarized everywhere (other choices for the relative orientations of \mathbf{m}_0 and \mathbf{B}_0 would change this). We immediately identify [23],

$$\begin{aligned}
\hat{\mathbf{b}}(\mathbf{r}, \omega_L) &= -\hat{\boldsymbol{\rho}}, \quad \beta(\mathbf{r}, \omega_L) \equiv 0, \\
\alpha(\mathbf{r}, \omega_L) &= \frac{3m_0 \sin(2\theta)}{2r^3} \sqrt{1 + 4 \frac{r^4}{\delta_s(\omega_L)^4}} e^{-r/\delta_s(\omega_L)}, \quad (4.11)
\end{aligned}$$

$$\zeta(\mathbf{r}, \omega_L) = \operatorname{sgn}(\omega_L) \frac{r}{\delta_s(\omega_L)} + \arctan \left[\frac{2r^2}{\delta_s(\omega_L)^2} \right].$$

There is therefore, nevertheless, a nontrivial phase change between the oscillating dipole and the oscillating field that increases linearly with distance r from the source.

2. Voltage response

Equations (2.2) and (2.4) describe the build up, defined to start at time $t=0$, and subsequent decay of the precession angle. The unit vector

$$\begin{aligned}
\hat{\mathbf{B}}_T^+(\mathbf{r}, t) &= \cos(\omega t + \varphi - \zeta_T) \hat{\mathbf{b}}_T(\mathbf{r}, \omega_L) \\
&\quad - \sin(\omega t + \varphi - \zeta_T) \hat{\mathbf{B}}_0 \times \hat{\mathbf{b}}_T(\mathbf{r}, \omega_L) \quad (4.12)
\end{aligned}$$

is determined by (4.8) even for $t > \tau_p$: the continued precession of the magnetization in effect defines a direction for $\hat{\mathbf{B}}_T^+(\mathbf{r}, t)$ even after the transmitter current is shut off. One has then,

$$\partial_t \mathbf{M}_N(\mathbf{r}, t) = \omega_L |\mathbf{M}_N^{(0)}(\mathbf{r})| e^{-(t-\tau_p)/T_2(\mathbf{r})} \sin[\theta_T(\mathbf{r}, \tau_p)] \hat{\mathbf{B}}_T^+(\mathbf{r}, t), \quad (4.13)$$

where terms of relative $O(1/\omega_L T_1, 1/\omega_L T_2)$ have been neglected. Substituting this form into (2.21) and using (4.8) one obtains for $t > \tau_p$:

$$\begin{aligned}
V_R^N(t) &= -\frac{1}{2} \omega_L \int d^3 r |\mathbf{M}_N^{(0)}(\mathbf{r})| e^{-(t-\tau_p)/T_2(\mathbf{r})} \sin[\theta_T(\mathbf{r}, \tau_p)] \\
&\quad \times \left\{ e^{-i(\omega_L t + \varphi - \zeta_T)} (\hat{\mathbf{b}}_T - i\hat{\mathbf{B}}_0 \times \hat{\mathbf{b}}_T) \cdot \int_0^{t_{\max}} dt' e^{t'/T_2(\mathbf{r})} \right. \\
&\quad \times \mathcal{B}_R(\mathbf{r}, t') e^{i\omega_L t'} + e^{i(\omega_L t + \varphi - \zeta_T)} \\
&\quad \times (\hat{\mathbf{b}}_T + i\hat{\mathbf{B}}_0 \times \hat{\mathbf{b}}_T) \cdot \int_0^{t_{\max}} dt' e^{t'/T_2(\mathbf{r})} \\
&\quad \left. \times \mathcal{B}_R(\mathbf{r}, t') e^{-i\omega_L t'} \right\}, \quad (4.14)
\end{aligned}$$

in which the introduction of the maximum time t_{\max} , which lies somewhere in the pulse interval $t - \tau_p < t_{\max} < t$, recognizes the fact that the form (4.13) for the rate of change of the magnetization is valid only after the transmitter field is turned off. The reason one must be careful here is that the memory function $\mathcal{B}_R(\mathbf{r}, -t')$ decays for large t' as a slow power law [see, e.g., (3.6), where a $t'^{-5/2}$ decay is exhibited for a point dipole receiver], whereas the e^{t'/T_2} factor grows exponentially. The latter will then overwhelm the former at late times. Physically this means that the late time decay of the signal will actually be governed not by the late time T_2 decay of the magnetization, but by the late arrival of the *tail* of the diffusing signal coming from the *early time* magnetization dynamics. This effect, which will be quantified in more detail in the next subsection, is extremely important to the measurement of T_2 . If, however, one is interested only in the voltage signal in the regime $\tau_d \ll t - \tau_p \ll T_2$, one may safely drop all of the T_2 exponentials. It is then safe to take the limit $t_{\max} \rightarrow \infty$ and one obtains,

$$\begin{aligned}
V_R^N(t) &= -\frac{1}{2} \omega_L \int d^3 r |\mathbf{M}_N^{(0)}(\mathbf{r})| \sin[\omega_T(\mathbf{r}) \tau_p] \\
&\quad \times \{ e^{-i(\omega_L t + \varphi - \zeta_T)} \mathcal{B}_R(\mathbf{r}, \omega_L) \cdot [\hat{\mathbf{b}}_T(\mathbf{r}, \omega_L) - i\hat{\mathbf{B}}_0 \\
&\quad \times \hat{\mathbf{b}}_T(\mathbf{r}, \omega_L)] + e^{i(\omega_L t + \varphi - \zeta_T)} \\
&\quad \times \mathcal{B}_R(\mathbf{r}, -\omega_L) \cdot [\hat{\mathbf{b}}_T(\mathbf{r}, \omega_L) + i\hat{\mathbf{B}}_0 \times \hat{\mathbf{b}}_T(\mathbf{r}, \omega_L)] \}. \quad (4.15)
\end{aligned}$$

The last line is simply the complex conjugate of the previous line. Now, the output of a typical NMR experiment is not $V_R^N(t)$, but has the rapid oscillations at frequency ω_L removed. This is accomplished with a *quadrature detection* scheme [1] whose output is the (real and imaginary parts of the) complex envelope voltage,

$$\begin{aligned}
\bar{V}_R^N(t) &\equiv -\omega_L \int d^3 r |\mathbf{M}_N^{(0)}(\mathbf{r})| \sin[\omega_T(\mathbf{r}) \tau_p] \\
&\quad \times e^{i\zeta_T(\mathbf{r}, \omega_L)} \mathcal{B}_R(\mathbf{r}, \omega_L) \cdot [\hat{\mathbf{b}}_T(\mathbf{r}, \omega_L) - i\hat{\mathbf{B}}_0 \times \hat{\mathbf{b}}_T(\mathbf{r}, \omega_L)], \quad (4.16)
\end{aligned}$$

which is time independent in this short time regime. It is the quantity $\bar{V}_R^N(t)$ that is extrapolated back to $t = \tau_p^+$, and one then obtains the formal relation

$$V(q, \mathbf{x}_0) \equiv \bar{V}_R^N(\tau_p^+) = \int d^3r K(q, \mathbf{x}_0; \mathbf{r}) n_N(\mathbf{r}), \quad (4.17)$$

in which $n_N(\mathbf{r})$ is the number density of (detectable) nuclear spins [$= 2n(\mathbf{r})$ for water, where $n(\mathbf{r})$ is the molecular number density], $\mathbf{x}_0 = (x_0, y_0)$ labels the horizontal position of the receiver loop, and the integration kernel is given by

$$\begin{aligned} K(q, \mathbf{x}_0; \mathbf{r}) \equiv & - \frac{\omega_L \gamma^2 \hbar^2 S(S+1) B_0}{3k_B T} \sin \left\{ \frac{1}{2} \gamma q [\alpha_T(\mathbf{r}, \omega_L) \right. \\ & \left. - \beta_T(\mathbf{r}, \omega_L)] \right\} e^{i\zeta_T(\mathbf{r}, \omega_L)} \\ & \times \mathcal{B}_R(\mathbf{r}, \omega_L) \cdot [\hat{\mathbf{b}}_T(\mathbf{r}, \omega_L) - i\hat{\mathbf{B}}_0 \times \hat{\mathbf{b}}_T(\mathbf{r}, \omega_L)]. \end{aligned} \quad (4.18)$$

This again confirms that it is indeed only the pulse moment $q = I_T^0 \tau_p$ that enters the response.

Now, from (2.14), $\mathcal{B}_R(\mathbf{r}, \omega_L)$ is simply the magnetic field generated by a unit current $e^{-i(\omega_L t + \phi)}$ in the receiver coil oscillating at the Larmor frequency ω_L . The orthogonal components of this field may also be written in a form analogous to (4.2) [due to the dot product in (4.18), it is only these components that enter]:

$$\begin{aligned} \mathcal{B}_R^\perp(\mathbf{r}, \omega_L) = & e^{i\zeta_R(\mathbf{r}, \omega_L)} [\alpha_R(\mathbf{r}, \omega_L) \hat{\mathbf{b}}_R(\mathbf{r}, \omega_L) \\ & + i\beta_R(\mathbf{r}, \omega_L) \hat{\mathbf{B}}_0 \times \hat{\mathbf{b}}_R(\mathbf{r}, \omega_L)]. \end{aligned} \quad (4.19)$$

The generalization of (2.35) is then

$$\begin{aligned} K(q, \mathbf{x}_0; \mathbf{r}) = & - \frac{\omega_L \gamma^2 \hbar^2 S(S+1) B_0}{3k_B T} \sin \left\{ \frac{1}{2} \gamma q [\alpha_T(\mathbf{r}, \omega_L) \right. \\ & \left. - \beta_T(\mathbf{r}, \omega_L)] \right\} e^{i[\zeta_T(\mathbf{r}, \omega_L) + \zeta_R(\mathbf{r}, \omega_L)]} \\ & \times [\alpha_R(\mathbf{r}, \omega_L) + \beta_R(\mathbf{r}, \omega_L)] [\hat{\mathbf{b}}_R(\mathbf{r}, \omega_L) \cdot \hat{\mathbf{b}}_T(\mathbf{r}, \omega_L) \\ & + i\hat{\mathbf{B}}_0 \cdot \hat{\mathbf{b}}_R(\mathbf{r}, \omega_L) \times \hat{\mathbf{b}}_T(\mathbf{r}, \omega_L)]. \end{aligned} \quad (4.20)$$

Note that it is the *corotating* part of the transmitted field and (due to the time-reversed nature of the adjoint field) the *counterrotating* part of the receiver field that enters the voltage response. The former determines the tipping angle while the latter determines the response amplitude. In the adiabatic limit, $\zeta_{T,R}, \beta_{T,R} \rightarrow 0$, $\alpha_{T,R} \rightarrow |\mathcal{B}_{T,R}^{0+}|$, $\hat{\mathbf{b}}_{T,R} \rightarrow \hat{\mathbf{b}}_{T,R}^0$, and (2.35) is recovered. When the transmitter and receiver loops coincide (4.20) reduces to the form

$$\begin{aligned} K(q, \mathbf{x}_0; \mathbf{r}) = & - \frac{\omega_L \gamma^2 \hbar^2 S(S+1) B_0}{3k_B T} e^{2i\zeta_T(\mathbf{r}, \omega_L)} \quad (4.21) \\ & \times \sin \left\{ \frac{1}{2} \gamma q [\alpha_T(\mathbf{r}, \omega_L) - \beta_T(\mathbf{r}, \omega_L)] \right\} \\ & \times [\alpha_T(\mathbf{r}, \omega_L) + \beta_T(\mathbf{r}, \omega_L)] \end{aligned}$$

$$\begin{aligned} = & - \frac{2\omega_L \gamma^2 \hbar^2 S(S+1) B_0}{3k_B T I_T^0} e^{2i\zeta_T(\mathbf{r}, \omega_L)} \\ & \times |\mathcal{B}_T^-(\mathbf{r}) \sin(\gamma \tau_p |\mathcal{B}_T^+(\mathbf{r})|), \end{aligned}$$

in which, in the second line we have introduced the physical corotating and counterrotating parts of the transmitted field. In the adiabatic limit both have the same amplitude, equal to half the total field amplitude, and (2.37) is recovered.

Notice that if the transmitter and receiver coils are *not* coincident, the kernel K , through its real and imaginary parts, is independently sensitive to the components of the magnetization parallel and perpendicular to the polarization vector $\hat{\mathbf{b}}_T$. This is true in both the adiabatic and nonadiabatic cases, and may provide some motivation for considering noncoincident loop geometries. For coincident geometries the adiabatic response voltage (2.37) is real. Adiabatic corrections lead to phase changes in the subsurface transmitter and receiver fields, and, even for coincident loops, this produces a complex phase factor $e^{2i\zeta_T}$ in the response voltage (4.21). The relative size of the ‘‘quadrature component,’’ i.e., of the imaginary part of the response voltage, is then a direct experimental measure of the breakdown of the adiabatic limit [24]. Since ζ_T varies with depth, the overall phase of the voltage signal will be a nontrivial function of the pulse moment q . The fact that the phase comes in doubled is significant: from the analytic model discussed in Sec. IID and at the end of Sec. IV A 1, one expects this phase to increase linearly with distance from the transmitter loop. Thus, for example, if $r/\delta_s(\omega_L) \simeq \pi/4$ one expects the contribution to the voltage to be approximately 90° out of phase, i.e., purely quadrature. Measurable interference effects between different subsurface regions should then be observable at depths much less than the skin depth. In Sec. V numerical results using the kernel (4.21) will be presented that support this conjecture.

3. Voltage response at long times

Equation (4.15) was derived from (4.14) by assuming that $t < T_2$. Imagine for a moment that $T_2 < 0$. Then convergence as $t \rightarrow \infty$ is ensured, and one obtains (4.15) and (4.16) for all times $t \gg \tau_d + \tau_p$, but with the replacement $\mathcal{B}_R(\mathbf{r}, \pm \omega_L) \rightarrow e^{-(t-\tau_p)/T_2} \mathcal{B}_R(\mathbf{r}, \pm \omega_L - i/T_2(\mathbf{r}))$, where $\mathcal{B}_R(\mathbf{r}, \pm \omega_L - i/T_2(\mathbf{r}))$ is the analytic continuation of $\mathcal{B}_R(\mathbf{r}, \pm \omega_L)$ to complex frequencies. Now, although the integral no longer converges when $T_2 > 0$, the analytic continuation remains perfectly well defined. It can then be shown that if one is interested only in the part of the signal that oscillates at the Larmor frequency, both (4.15) and (4.16) remain valid, with this same replacement. Unfortunately, this portion of the signal, which continues to decay exponentially on the time scale T_2 , becomes subdominant at large t to an essentially *dc* signal that decays as a slow power law. It is the purpose of this subsection to understand the origin of this signal and the information it contains.

In analyzing the long-time decay of the voltage response, one must take care to consider the contributions from all possible sources. Thus, in addition to the contributions from the nuclear spins, there will also be contributions from currents induced in the ground *directly* by the transmitter loop.

It is the late time arrival of the diffusive tail of all such signals that gives rise to the slowly decaying dc power law.

From (2.19), following the same steps used to derive (2.21), one may write the total voltage response in the form

$$V_R(t) = -\partial_t \int d^3r \int_0^\infty \mathcal{B}_R(\mathbf{r}, t') \cdot [\mathbf{M}(\mathbf{r}, t-t') - \mathbf{M}_0(\mathbf{r})], \quad (4.22)$$

where $\mathbf{M} = \mathbf{M}_N + \mathbf{M}_T + \mathbf{M}_R$ is the total magnetization density, with $\mathbf{j} = c \nabla \times \mathbf{M}$. The total equilibrium background magnetization, which clearly makes no contribution to the voltage response, has been subtracted for convergence purposes. For a horizontal loop, the magnetization is vertical, uniform across the area of the loop, with magnitude $I(t)/c$, where $I(t)$ is the current in the loop. Now, the transmitter loop current runs only during the pulse time interval $0 \leq t < \tau_p$, and the nuclear magnetization response builds up over this same time interval, then decays exponentially back to its equilibrium value on the time scale T_2 . The receiver loop current, since it provides the measured response to all the fields generated in the ground by the NMR apparatus, will decay with the same slow power law that the fields do. However the magnitude of the receiver current is presumed to be tiny, and this self-inductance effect should be negligible compared to the effects of j_T and j_N in all regimes of interest. The time integration in (4.22) is then essentially restricted to a finite time interval. At large times, compared to the diffusion time τ_d across the measurement region [a fraction of a millisecond in typical situations—see (2.24)], one will have the asymptotic form

$$\mathcal{B}_R(\mathbf{r}, t') \approx \mathcal{B}_R^\infty(\mathbf{r}) \frac{1}{\tau_d} \left(\frac{\tau_d}{t'} \right)^p \quad (4.23)$$

with $p = 5/2$ [see, e.g., Eq. (3.6)]. The $1/\tau_d$ prefactor is chosen so that \mathcal{B}_R^∞ has the same units as \mathcal{B}_R^0 in (2.29), i.e., magnetic field per unit current. Thus \mathcal{B}_R^∞ should be of the same order as \mathcal{B}_R^0 . Let t_{\max} be the time beyond which all contributions to $\mathbf{M} - \mathbf{M}_0$ effectively vanish (thus $t_{\max} = \tau_p$ for \mathbf{M}_T , while $t_{\max} - \tau_p \gg T_1, T_2$ for \mathbf{M}_N). One obtains then for $t > t_{\max} + \tau_d$,

$$V_R(t) \approx \frac{p}{\tau_d^2} \left(\frac{\tau_d}{t} \right)^{p+1} \int d^3r \mathcal{B}_R^\infty(\mathbf{r}) \cdot \int_0^{t_{\max}} ds \frac{\mathbf{M}(\mathbf{r}, s) - \mathbf{M}_0(\mathbf{r})}{(1-s/t)^{p+1}}. \quad (4.24)$$

Since τ_d is so small in typical situations, this form obtains almost immediately after the magnetization returns to its equilibrium value. Suppose now that $t/t_{\max} \gg 1$. One may then drop the denominator in the time integral to obtain the pure power law form,

$$V_R(t) \approx \frac{p}{\tau_d^2} \left(\frac{\tau_d}{t} \right)^{p+1} \int d^3r \mathcal{B}_R^\infty(\mathbf{r}) \cdot \mathcal{M}(\mathbf{r}), \quad (4.25)$$

in which

$$\mathcal{M}(\mathbf{r}) \equiv \int_{-\infty}^{\infty} ds [\mathbf{M}(\mathbf{r}, s) - \mathbf{M}_0(\mathbf{r})] \quad (4.26)$$

is the total integrated magnetization pulse. Note that in this limit all contributions from the subdominant exponentially decaying Larmor frequency terms disappear.

Let us consider various experimentally motivated model forms for \mathcal{M} . The transmitter loop magnetization takes the form $\mathbf{M}_T(\mathbf{r}, t) = \hat{\mathbf{n}} [I_T(t)/c] \delta(z) \chi_T(\mathbf{r})$, where $\hat{\mathbf{n}} = \pm \hat{\mathbf{z}}$ is the loop normal (for a figure-eight loop the normal is $\hat{\mathbf{z}}$ on one lobe and $-\hat{\mathbf{z}}$ on the other), and the indicator function $\chi_T(\mathbf{r})$ is unity inside the area of the loop and vanishes outside. For the current we take the model form $I_T(t) = I_T^0 E_T(t) \cos(\omega_L t + \varphi)$, where $E_T(t)$ is an envelope function given roughly by $E_T(t) \approx \theta(t) \theta(\tau_p - t)$. The contribution to (4.24) from the transmitter loop then takes the form

$$\begin{aligned} \mathcal{M}_{M,T}(\mathbf{r}) &= \frac{1}{c} I_T^0 \hat{\mathbf{z}} \delta(z) \chi_T(\mathbf{r}) \int_{-\infty}^{\infty} ds E_T(s) \cos(\omega_L s + \varphi) \\ &\approx I_T^0 \hat{\mathbf{z}} \delta(z) \chi_T(\mathbf{r}) \frac{\sin(\omega_L \tau_p + \varphi) - \sin(\varphi)}{\omega_L c}, \end{aligned} \quad (4.27)$$

where the second line follows from the square pulse choice for the envelope function. The combination $I_T^0 \mathcal{B}_R^\infty$ is of order the amplitude of the tipping field, i.e., about 10^{-2} G. Using a loop radius of $R = 50$ m and, from (2.24), $\tau_d \sim 0.1$ ms, one may therefore estimate the corresponding contribution to the voltage as $V_R \sim (10^{-8} c) p I_T^0 |\mathcal{B}_R^\infty| \pi R^2 / \tau_d^2 \omega_L c (\tau_d/t)^{p+1} \sim 1 \mu\text{V} (\tau_d/t)^{p+1}$. This estimate should be valid a few Larmor periods after the end of the tipping pulse, and therefore becomes immeasurably small on the time scale T_2 of the Larmor frequency signal. Note also the extreme sensitivity of this result to τ_p . In particular, it can be made to vanish identically if $\omega_L \tau_p$ is chosen, for any integer n to be either of the form $2n\pi$ or of the form $(2n+1)\pi - 2\varphi$. A similar result will hold for any choice of envelope function. Since the precise nature of the envelope function (as well as the precise value of the phase φ) is experimentally uncontrollable on the time scale $t_L = 2\pi/\omega_L$ (a fraction of a millisecond) of the Larmor period, the result (4.26) will basically be random from measurement to measurement, and will average to zero over a series of measurements. This average will then leave only contributions from the corrections to (4.24) that decay with the subleading power law $1/t^{p+2}$.

Similar considerations apply to the subsurface nuclear magnetization (2.4). The magnetization in the plane orthogonal to \mathbf{B}_0 has an envelope that ramps up from zero on the interval $0 \leq t < \tau_p$, then decays to zero exponentially on the time scale T_2 . However, this envelope is multiplied by a vector in the plane that rotates rapidly at the Larmor frequency. The result is then again a small, essentially random, integrated moment that averages to zero over a series of measurements. On the other hand, the magnetization along \mathbf{B}_0 does not oscillate, and hence does yield a net systematic pulse. The contribution to (4.25) is given by

$$\begin{aligned} \mathcal{M}_{M,N}(\mathbf{r}) &= \mathbf{M}_N^{(0)}(\mathbf{r}) \int_{-\infty}^{\infty} ds E_N(s) \\ &= -\mathbf{M}_N^{(0)}(\mathbf{r}) \left(\frac{1}{\omega_T(\mathbf{r})} \{ \omega_T(\mathbf{r}) \tau_p - \sin[\omega_T(\mathbf{r}) \tau_p] \} \right. \\ &\quad \left. + \{ 1 - \cos[\omega_T(\mathbf{r}) \tau_p] \} T_1(\mathbf{r}) \right), \end{aligned} \quad (4.28)$$

in which, motivated by the form (2.4), the second line follows from the choice of envelope function

$$E_N(t) = \begin{cases} 0, & t < 0 \\ \cos[\omega_T(\mathbf{r})t] - 1, & 0 \leq t < \tau_p \\ \{\cos[\omega_T(\mathbf{r})\tau_p] - 1\} e^{-(t-\tau_p)/T_1(\mathbf{r})}, & t \geq \tau_p, \end{cases} \quad (4.29)$$

where, for simplicity, we have taken $\tau_l = \tau_p$ [for $\tau_p \ll T_1$, a different choice for τ_l leads to subleading corrections to (4.28)]. This is a very interesting result. It says that after the Larmor frequency oscillations die out, with appropriate signal averaging, a slow dc power law decay is left over, which depends only on the decay of the parallel component of the nuclear magnetization. If T_1 is significantly larger than τ_p [as is really required for the validity of (2.4)], the last term in (4.28) dominates. Thus, if the nuclear magnetization is extracted from the usual NMR signal at short times via (4.17) and then used as an input into (4.28) and (4.25), an independent measure of the distribution of time constants $T_1(\mathbf{r})$ is obtained. A standard technique used by borehole NMR tools for measuring T_1 involves pulsing the *static* field \mathbf{B}_0 for varying lengths of time, and then using the NMR technique to measure the resulting buildup of the nuclear magnetization [25]. This method clearly cannot be implemented if the Earth's field is being used.

Finally, let us consider expected orders of magnitude. Consider first the level of the dc part of the signal *during* the magnetization pulse, $t < t_{\max}$. Since the magnetization along \mathbf{B}_0 varies slowly on the scale of τ_d , the adiabatic limit of (4.22) obtains, and from (2.27) one has simply

$$V_R^{\text{dc}}(t) = - \int d^3r \hat{\mathbf{B}}_0 \cdot \mathcal{B}_R^0(\mathbf{r}) \hat{\mathbf{B}}_0 \cdot \partial_t \mathbf{M}_N(\mathbf{r}, t). \quad (4.30)$$

The order of magnitude of this signal may be estimated simply by noting that it will be roughly a factor $\omega_L T_1$ smaller than the amplitude of the Larmor signal [see the discussion below (2.37)]. For $T_1 \sim 100$ ms one then finds $V_R^{\text{dc}} \sim 1$ nV, an immeasurably small value. The magnitude of this signal for $t > t_{\max}$ will then be reduced from this by a factor $[\tau_d / (t - t_{\max})]^{p_{\text{eff}}}$, where $p < p_{\text{eff}} < p + 1$ is some effective power mimicking the behavior of (4.24) at intermediate times before (4.25) becomes valid, and will therefore also be unobservable. For completeness, and in the hope that some form of future experiment may access this regime, it is nevertheless worthwhile performing the estimate in the regime in which (4.25) is valid. The prefactor is of order $(T_1 / \tau_d)^2$ times the above estimate for V_R^{dc} . The diffusion time is estimated in (2.24). With $L = 50$ m and $\rho = 10$ Ω m, one finds $\tau_d = 0.1$ ms. Thus $(T_1 / \tau_d)^2 \sim 10^6$ and we obtain $V_R \sim 1$ mV $(\tau_d / t)^{p+1}$. Note that the prefactor here is three orders of magnitude larger than the corresponding prefactor computed above for the direct contribution due to the transmitter loop. However, since this form is valid only for $t \gg T_1$, one still finds V_R in the immeasurably small femtovolt range.

Extraction of the nuclear magnetic contribution to the coefficient of $1/t^{p+1}$ from the experiments considered in this work is impossible. Nevertheless, application of (4.25) to future laboratory experiments performed under more favorable conditions may be possible, and in principle the infor-

mation content of such a measurement is intriguing. Note that measuring the response of the ground to an electromagnetic pulse is a common field technique for determining its conductivity structure. In Eq. (4.27) the pulse is coming from the nuclear spins themselves, but the unknown distribution of $T_1(\mathbf{r})$ precludes an independent extraction of the conductivity structure.

B. The inverse problem

Given a model of the electromagnetic characteristics of the subsurface, (4.17) with (4.20) or (4.21) represents an equation for the voltage response (actually, two equations for the real and imaginary parts of the voltage response) due to a given subsurface water distribution. One is actually interested in the inverse problem, i.e., inferring the nuclear spin distribution from a series of voltage measurements. This distribution is in general fully three-dimensional, and solving this inverse problem, even in principle, would then require measurements at many different loop positions \mathbf{x}_0 , as well pulse moments q . Typically, however, \mathbf{x}_0 is held fixed and only q is varied. In this case only certain spatial averages of the water distribution can be inferred. Only if a horizontally stratified subsurface structure is assumed can one in principle recover full information. As computation of the magnetic fields entering (4.6) is tractable only in this latter case, we shall make this assumption in all that follows.

With a horizontally stratified conductivity structure, the kernel $K(q, \mathbf{x}_0; \mathbf{r})$ is actually translation invariant in the horizontal position \mathbf{x}_0 . Writing $\mathbf{r} = (\mathbf{x}, z)$ with $\mathbf{x} = (x, y)$, this means that $K = K(q, \mathbf{x}_0 - \mathbf{x}; z)$. Let

$$\hat{K}(q, \mathbf{k}; z) = \int d^2x_0 e^{i\mathbf{k} \cdot (\mathbf{x}_0 - \mathbf{x})} K(q, \mathbf{x}_0 - \mathbf{x}; z) \quad (4.31)$$

be the horizontal Fourier transform of the kernel, and let

$$\hat{n}_N(\mathbf{k}, z) = \int d^2x n_N(\mathbf{x}, z) e^{i\mathbf{k} \cdot \mathbf{x}}, \quad (4.32)$$

$$\hat{V}_N(q, \mathbf{k}) = \int d^2x_0 V_N(q, \mathbf{x}_0) e^{i\mathbf{k} \cdot \mathbf{x}}$$

be the corresponding horizontal Fourier transforms of the nuclear spin density and of the response voltage. Equation (4.17) then becomes

$$\hat{V}(q; \mathbf{k}) = \int dz \hat{K}(q, \mathbf{k}; z) \hat{n}_N(\mathbf{k}, z). \quad (4.33)$$

The full three-dimensional problem therefore separates into a separate one-dimensional problem for each individual value of \mathbf{k} . For the inverse problem, $V(q; \mathbf{k})$ must be computed approximately from a series of measurements of $V(q; \mathbf{x}_0)$ for a sequence of q 's at different points \mathbf{x}_0 . If $n_N = n_N(z)$ is horizontally translation invariant, i.e., independent of \mathbf{x} , then $\hat{n}_N(\mathbf{k}, z) = n_N(z) (2\pi)^2 \delta(\mathbf{k})$, and only the $\mathbf{k} = 0$ equation survives.

Typically one simply measures $V(q; \mathbf{x}_0)$ at a fixed point \mathbf{x}_0 and *assumes* that $n_N \equiv \hat{n}_N(\mathbf{x}_0; z)$ is independent of \mathbf{x} . One therefore inverts the relation

$$V(q; \mathbf{x}_0) = \int dz \hat{K}(q, \mathbf{0}; z) \tilde{n}_N(\mathbf{x}_0; z), \quad (4.34)$$

for the function $\tilde{n}_N(z)$. However, as the notation indicates, if the water distribution is *not* horizontally translation invariant, the water density inferred in this way will change if the loop position \mathbf{x}_0 is changed. The relation between the exact $n_N(\mathbf{x}, z)$ and $\tilde{n}_N(\mathbf{x}_0; z)$ may be obtained by writing (4.17) in the form

$$V(q; \mathbf{x}_0) = \int dz \hat{K}(q, \mathbf{0}; z) \int d^2x \frac{K(q, \mathbf{x}_0 - \mathbf{x}; z)}{\hat{K}(q, \mathbf{0}; z)} n_N(\mathbf{x}, z). \quad (4.35)$$

Thus we identify

$$\tilde{n}_N(\mathbf{x}_0; z) = \int d^2x \frac{K(q, \mathbf{x}_0 - \mathbf{x}; z)}{\hat{K}(q, \mathbf{0}; z)} n_N(\mathbf{x}, z), \quad (4.36)$$

which is then a convolution of the true density with the normalized kernel. Thus $\tilde{n}_N(\mathbf{x}_0; z)$ is a nontrivial, horizontally weighted average of $n_N(\mathbf{r}, z)$. In the context of the inverse problem, the relation (4.36) demonstrates that there are strong hidden correlations between \tilde{n}_N and the kernel K that are not evident in (4.34). These correlations become evident only if one attempts to invert (4.36) for the actual $n_N(\mathbf{x}, z)$ based on a sequence of $\tilde{n}_N(\mathbf{x}_0; z)$ at different \mathbf{x}_0 . One may find instabilities in this second inversion that could be avoided by performing a careful simultaneous inversion in q and \mathbf{x}_0 based on the Fourier representation (4.34).

For the purposes of the present paper, we shall deal with strictly one-dimensional model inverse problems based on the one-dimensional kernel (4.34). In Sec. VB the structure of this kernel will be investigated numerically, and in Sec. VC the associated inverse problem will be investigated for various model data sets with special attention to the effects of finite ground conductivity.

V. NUMERICAL SIMULATIONS

Equations (4.17) and (4.20) completely specify the solution to the forward problem for the NMR response voltage for a typical NMR experiment. Kernels similar to Eq. (4.21), for coincident receiver and transmitter loops, have already appeared in the geophysical literature (see, e.g., [4–6,17]), but these earlier works accounted either incorrectly or not at all for the effect of a finite conductivity structure. In this section the nature of the more general forward theory described in this work is characterized by presenting computations performed in geophysically relevant settings. We especially contrast the results with predictions made for the adiabatic limit in which the medium of propagation is an effective insulator. In addition, synthetic inversions are presented that demonstrate the importance of utilizing the more general theory in inferring information about the density and spatial distribution of water. Optimally, we would also have liked to present inversions of real experimental NMR data. Unfortunately this is a pointless exercise unless the NMR data is accompanied by ground truth. Thus, a proper experimental evaluation of the theory requires coincident *direct*

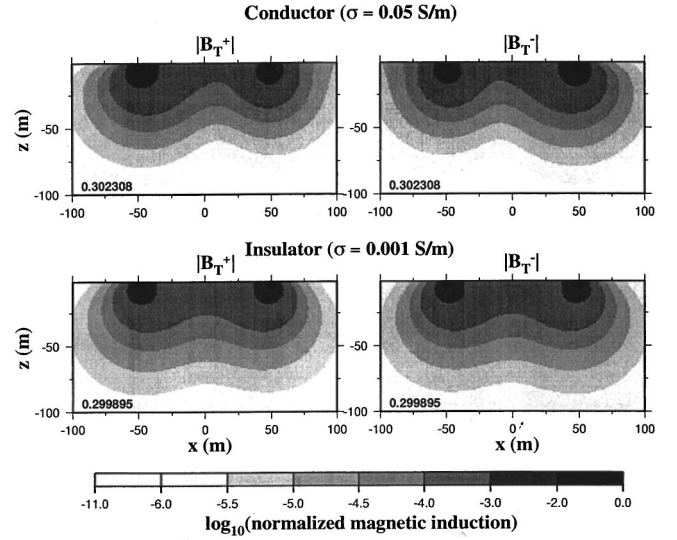


FIG. 1. An east-west ($y=0$) oriented vertical (x - z) slice of the magnitude of the applied corotating ($|\mathbf{B}_T^+|$, left column) and counterrotating ($|\mathbf{B}_T^-|$, right column) fields for a conductor ($\sigma=0.05$ S/m, top row) and an effective insulator ($\sigma=10^{-3}$ S/m, taken slightly nonzero for numerical convenience, bottom row). The orientation of the static field is described in the text. For an insulator, the corotating and counterrotating fields are both equal to exactly half the amplitude of the applied tipping field at each point and are symmetric around $x=0$. Appreciable conductivity breaks the symmetry slightly causing the corotating and counterrotating fields to differ from one another, although each is just the mirror reflection of the other through the y - z plane. The fields are normalized by the maximum value indicated in the bottom left corner of each subplot, units are Gauss/Amp, and the gray scale is logarithmic.

ground-water measurements (e.g., via a well or borehole) with which to compare to the NMR inversion. To further complicate matters, ground truth would also have to involve an independent measure of the ground conductivity structure, as well as the porosity and magnetic impurity concentration level of the ground at each depth. Since T_1 and T_2 are strongly dependent on the latter properties [15], they are required to estimate the extent to which the water in each region is actually visible in the NMR signal. Although many NMR ground-water surveys have been performed, none (that we know of, or have access to) were performed in the presence of the required ground truth. We are currently working on proposals to fill this gap, both with laboratory and geophysical measurements. In the present work we are then limited to comparisons with synthetic data. In addition, we treat here only the relatively simple case of a uniformly conducting half-space. We will present a detailed investigation of the effects of more complicated horizontally stratified conductivity structures in future work [19].

To simplify the simulations, we have imposed the following conditions and assumptions: the Earth's static field is assumed to have a magnitude of 0.587 G (consistent with a Larmor frequency of 2500 Hz) pointing north at an angle of 25° from the vertical (declination 0°E and inclination of 65°N), the circular receiver and transmitter loops are coincident with a diameter of 100 m, and the solid Earth is a homogeneous conducting half-space. Varying the inclination of the static field changes the results in detail (varying the

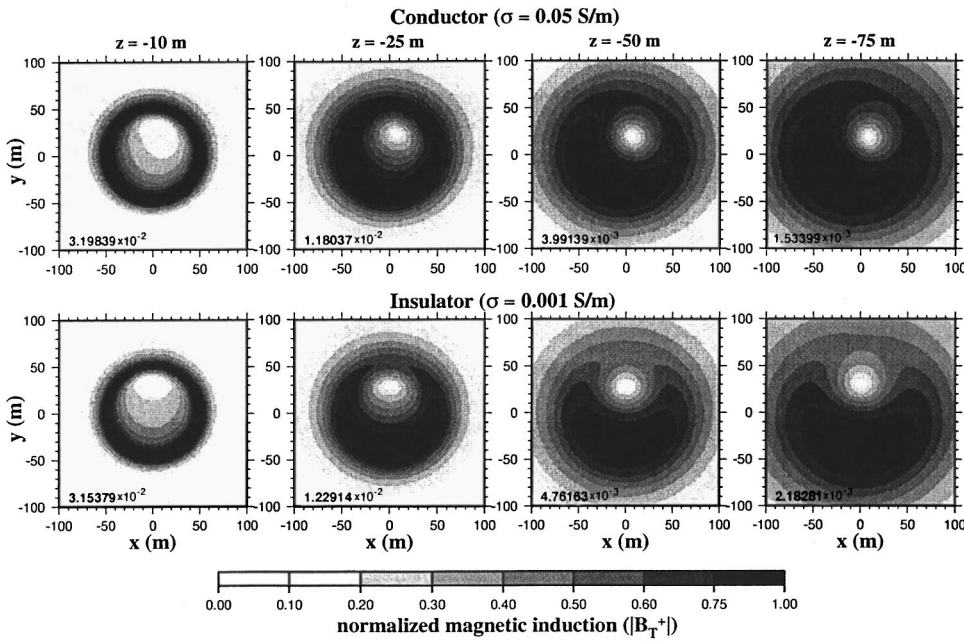


FIG. 2. Same as Fig. 1, but here horizontal (x - y) slices of the magnitude of the field are presented at different specified depths, z . Only the corotating field ($|\mathbf{B}_T^+|$) is shown due to the mirror symmetry apparent in Fig. 1. The gray scale is not logarithmic.

inclination serves only to rotate the coordinate system), but the general conclusions drawn from the simulations will be unaffected. Genuinely realistic simulations, however, would require conductivity to be a variable function of depth, particularly because it is a strong function of water content. It should be emphasized that (4.17), (4.20), and (4.21) are formally valid for conductivity structures that can vary arbitrarily in three dimensions, but since the general effect of conductivity on the NMR response of a conductive medium can be demonstrated with a homogeneous half-space, for the purposes of the present work we have confined our numerical discussion to this simple case. More detailed inversions, in particular, need to be performed in the presence of stratified conductivity structures and for variable loop geometries.

A. The forward problem in three dimensions

The purpose of the forward simulations presented in this subsection is to illuminate the general theory in a geophysically realistic setting by demonstrating the character and importance of the effects of a conducting subsurface. For coincident transmitter and receiver loops, the complex NMR three-dimensional integral kernel is given by Eq. (4.21). Figures 1–9 present slices of the various fields that enter this kernel as well as the kernel itself. Throughout these figures, we contrast the values for an effective insulator with conductivity $\sigma = 0.001$ S/m (chosen slightly nonzero for numerical convenience) with that of an intermediate conductor with $\sigma = 0.05$ S/m. This value is fairly typical of dry, near-surface soils and sediments that have conductivities ranging from about $\sigma = 10^{-1} - 10^{-2}$ S/m. Highly porous water saturated sediments with alkaline entrained waters can have much higher conductivities ranging from fractional to several s/m. Thus, the effects of conductivity shown in Figs. 1–9 are of intermediate magnitude relative to those expected in near surface exploratory NMR surveys.

The Cartesian coordinate system that we use in the simulations has the positive x , y , and z axes in the east, north, and up directions, respectively. The circular coincident transmit-

ter and receiver coils, both with a radius of 50 m, lie on the Earth's surface, $z = 0$, and are centered at $\mathbf{x}_0 = (x, y) = (0, 0)$. The typical amplitude of the applied current in present instruments is $I_T^0 = 300$ A and tipping pulse lengths, $3 \text{ ms} < \tau_p < 30 \text{ ms}$, are chosen to produce pulse moments, $q = I_T^0 \tau_p$, ranging from 10^3 A-ms to 1.5×10^4 A-ms. In Figs. 3–9, a value $q = 10^4$ A-ms has been used. This is a relatively large

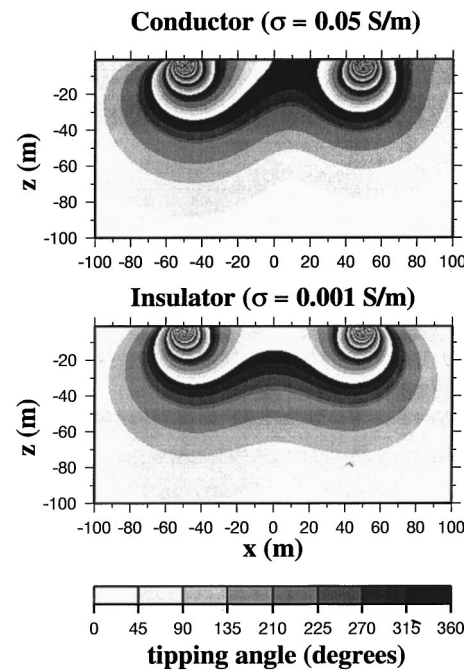


FIG. 3. An east-west ($y = 0$) oriented vertical (x - z) slice of the tipping angle, $\gamma\tau_p |\mathbf{B}_T^+(\mathbf{r})|$, for a conductor (top) and an effective insulator (bottom). The pulse moment chosen is $q = I_T^0 \tau_p = 10^4$ A-ms. The $\pm x$ asymmetry in the corotating applied field for the conductor, as shown in Fig. 1, manifests itself here as well. Excursions through 360° (jumps from black to white) indicate that the nuclear spins have been tipped full circle and returned to their initial orientations. Units are degrees, modulo 360.

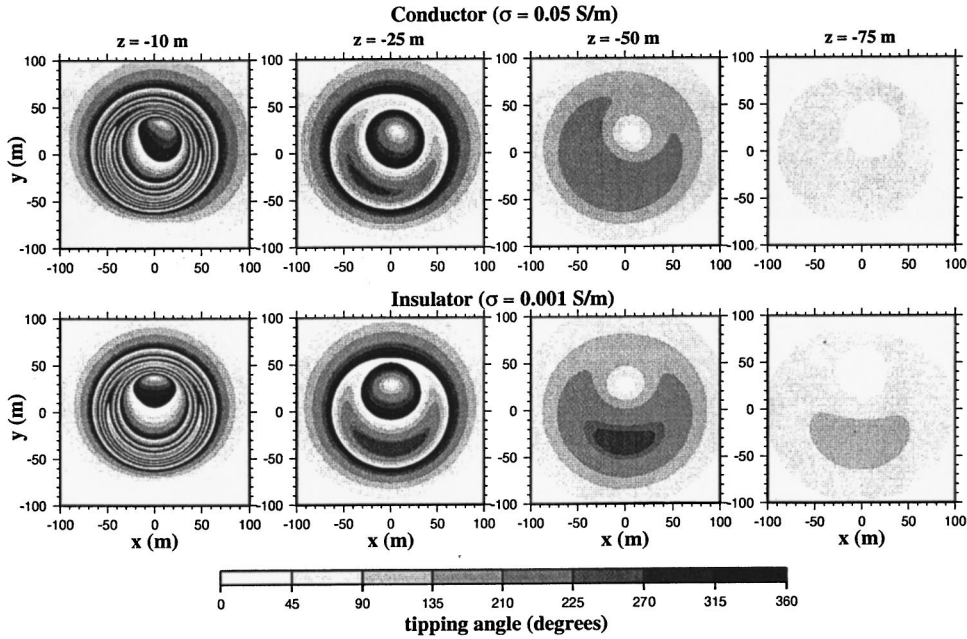


FIG. 4. Same as Fig. 3, but here horizontal (x - y) slices of the tipping angle are presented at different specified depths, z . Input parameters are described in the text.

value that substantially tips the spins at 100 m depth. The tipping field magnitudes shown in Figs. 1 and 2 are proportional to the current amplitude I_T^0 but are independent of the pulse length τ_p . The phase angles shown in Figs. 5 and 6 are independent of both I_T^0 and τ_p .

Figures 1 and 2 display various slices of the magnitude of the corotating ($|\mathbf{B}_T^+$) and counterrotating ($|\mathbf{B}_T^-$) components of the applied magnetic tipping field. These two fields differ from one another only in a conducting medium; for an insulator they are equal to half of the total applied field. The differences, however, are subtle, even for a conductor. As shown in Fig. 1, the conducting medium, of course, attenuates the applied field faster than does the effective insulator. More interestingly, the conducting medium exhibits a small $\pm x$ asymmetry not apparent in the effective insulator. The magnitudes of the corotating and counterrotating fields are mirror images of one another through the vertical plane containing the static field (the y - z plane in the figures). Mirror symmetry is restored only if the ground is insulating. Full axial symmetry exists if the Earth's field is precisely vertical.

The corotating applied tipping field controls the spatial distribution of the tipping angle, $\gamma\tau_p|\mathbf{B}_T^+|$, which is the argument of the sine in Eq. (4.21). Figures 3 and 4 show various slices of the tipping angle. Figures 1 and 2 are very similar to Figs. 3 and 4 because surfaces of fixed $|\mathbf{B}_T^+|$ obviously coincide with surfaces of fixed tipping angle. The main difference between these two sets of figures is that the tipping angles are defined only modulo 360° , which imparts a striping to Figs. 3 and 4. Instantaneous jumps from black to white represent the locations at which the spin direction has undergone one complete 360° orbit. Because the tipping angle is the argument of a sine, the magnitude of the imaging kernel maximizes for tipping angles of $\pm 90^\circ$. The differences between the tipping angles for the conductor and effective insulator are, again, subtle. Plots of tipping angles for different values of the pulse moment, q , are similar to Figs. 3 and 4 with one key exception. The magnitude of the tipping angle increases with q so that plots of tipping angles for $q < 10^4$ A-ms will be less oscillatory than those shown in Figs. 3 and

4 and significant tipping will be confined to shallower depths.

A much more significant effect of finite conductivity involves the variable ζ_T , half the phase lag between the received and transmitted signals from a particular point in space. As equation (4.21) shows, a nonzero ζ_T makes the NMR integral kernel complex. For a perfect insulator, $\zeta_T \equiv 0$ and the kernel is purely real. The complexity of the kernel dephases the transmitted and received voltages from different points in space. If $2\zeta_T$ is larger than about 20° , the NMR response of a conductive medium would significantly

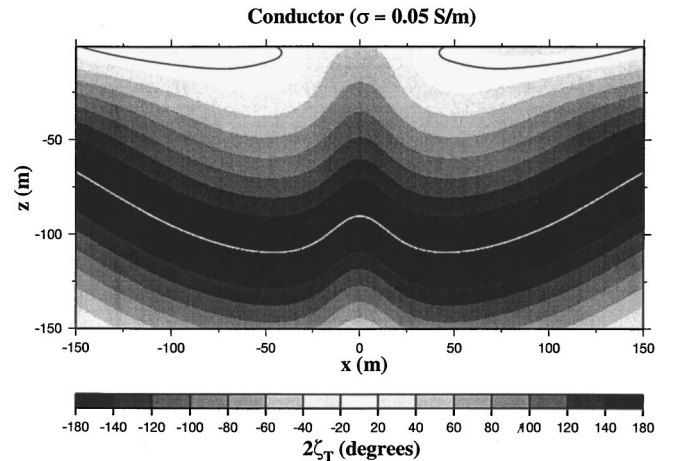


FIG. 5. An east-west ($y=0$) oriented vertical (x - z) slice of $2\zeta_T$, the phase lag between the transmitted and received signals from a particular point in space (the overall voltage is their linear superposition). The black lines, adjacent to the surface, mark the 0° contour, with positive values below it and negative values above it. The white line marks a $\pm 180^\circ$ contour with positive values above and negative values below it. The plot is mirror symmetric because ζ_T is effectively the same for both corotating and counterrotating parts of the applied field. The phase ζ_T is independent of both the transmitter current amplitude I_T^0 and the pulse length τ_p , and grows approximately linearly with distance from the coil. For an insulating medium the plot would be a featureless white: $\zeta_T \equiv 0$. Units are in degrees, and input parameters are described in the text.

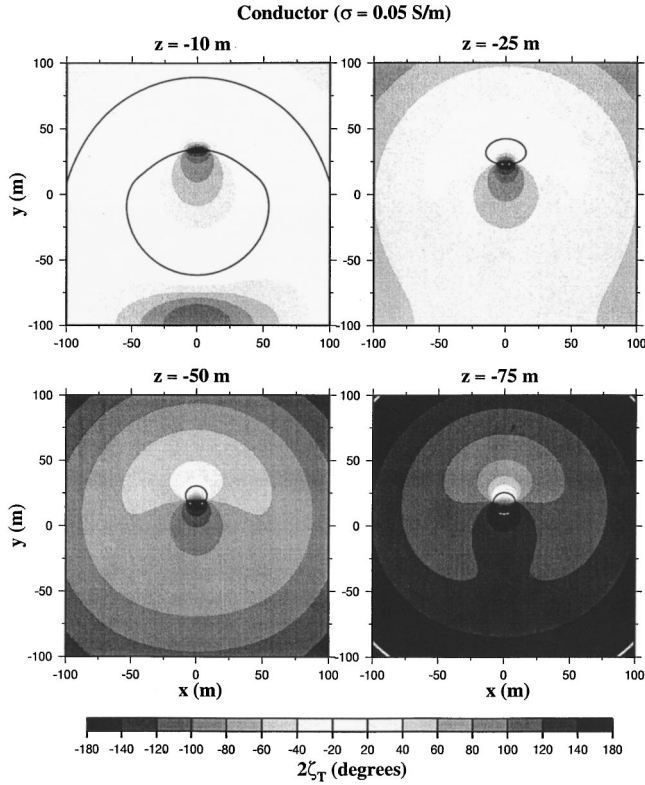


FIG. 6. Same as Fig. 5, but here horizontal (x - y) slices of $2\zeta_T$ are presented at different specified depths, z .

differ from the response of an insulator. As observed earlier, ζ_T is independent of both I_T^0 and τ_p , unlike the transmitted field or the tipping angle. It is then primarily a function of subsurface conductivity. As Figs. 5 and 6 demonstrate, $2\zeta_T \geq 20^\circ$ below about 20-m depth and reaches values as large as $\pm 180^\circ$ within the top 100 m, even for a relatively weak conductor ($\sigma = 0.05$ S/m). Unlike the tipping angle, ζ_T is effectively the same for both the co- and counter-rotating fields and hence does not exhibit $\pm x$ asymmetries. Its asymmetry in $\pm y$ is due to the inclination of the Earth's field.

The corotating and counterrotating applied tipping fields ($|B_T^+|$ and $|B_T^-|$) and the phase lag between the transmitted and received voltages ($2\zeta_T$) form the primary components of the complex integral kernel, $K(q, \mathbf{x}_0; \mathbf{r})$, in Eq. (4.21), and the geometrical distributions of these fields will control the nature of the NMR forward solution. Figures 7–9 display various slices of the real and imaginary parts of the three-dimensional integral kernels. The kernels exhibit $\pm x$ and $\pm y$ asymmetries derived from the applied fields and the tipping angle. The kernels for the conductor and the effective insulator are highly oscillatory, a characteristic inherited from the tipping angle, and are very similar near the surface where ζ_T is small and the conductive kernel is nearly real. The kernels become increasingly oscillatory as q increases. At greater depths, however, the kernels become much less oscillatory and the conductive kernel differs strongly from the insulating kernel, and develops a significant imaginary part. The real parts of the kernels may even have opposite sign. As discussed in Sec. VB below, the oscillatory nature of the kernels near the surface greatly diminishes the amplitude of this region's contribution to the NMR voltage because of massive cancellation upon integration against a

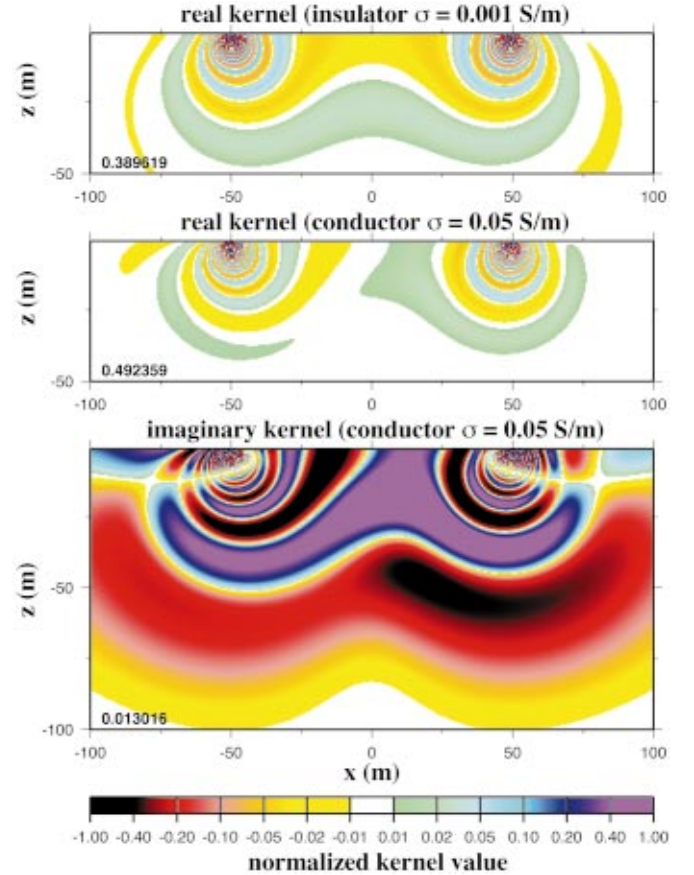


FIG. 7. (Color) An east-west ($y=0$) oriented vertical (x - z) slice of the three-dimensional integral kernel, $K(q, \mathbf{x}_0; \mathbf{r})$, of Eq. (4.21). The kernels are normalized by the maximum value indicated in the bottom left hand corner of each plot. Units are nV/m^3 [the definition in (4.17), which yields units of nV for the kernel, has been altered slightly by multiplying K by the bulk density of water]. Input parameters are described in the text.

smooth water distribution. Thus, it will be seen that even though the amplitudes of $K(q, \mathbf{x}_0; \mathbf{r})$ at depth are much smaller than those near the surface, the contribution of water content at depth may be as, or even more, important than in the shallow, near surface layers. This is clearly crucial if significant depth resolution is to be obtained from the solution to the inverse problem.

B. The forward problem for horizontally stratified water

It is clear from Figs. 7–9 that the imaging kernel has a tremendously complicated three-dimensional structure. The magnitude of the kernel is governed by the counterrotating applied tipping field ($|B_T^-|$), the pattern of oscillation by the sine of the tipping angle [$\sin(\gamma_{T_p})|B_T^+|$], and the ratio of real to imaginary parts governed by the phase lag ($2\zeta_T$) between the transmitted and received voltages. The kernel is largest and most oscillatory near the surface, purely real for an insulator (and nearly purely real for the effective insulator), and, increasingly with depth, develops a strong nonoscillatory imaginary part for the conductor. The prominent nearly horizontal sign change in the imaginary conductive kernel between depths of 10–20 m comes from the zero crossing of ζ_T (see Fig. 5). In order to simplify the analysis, in a manner

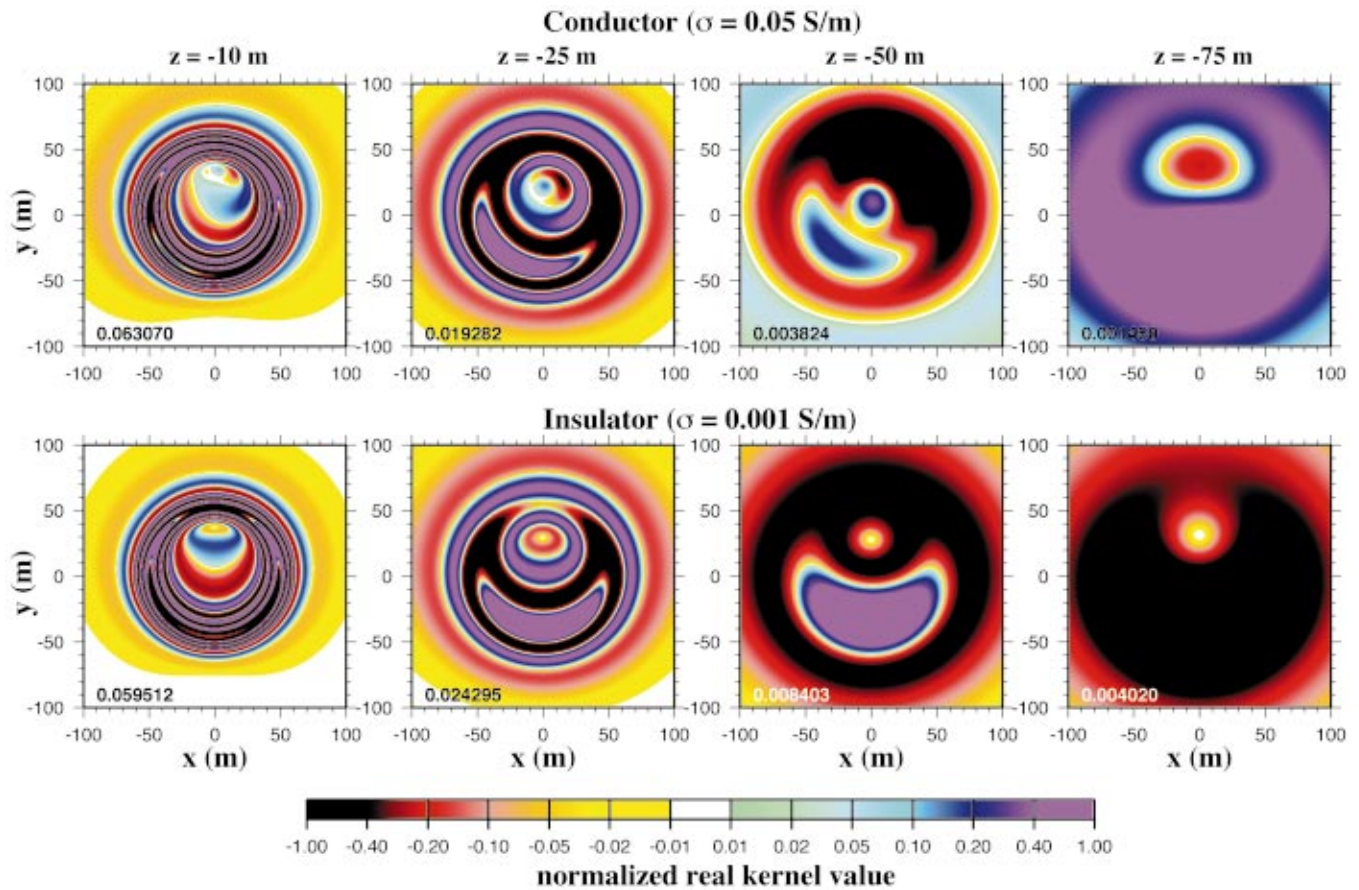


FIG. 8. (Color) Similar to Fig. 7, but here horizontal (x - y) slices of the real part of the kernel, $K(q, \mathbf{x}_0; \mathbf{r})$, are presented at different specified depths, z , for the effective insulator and the conductor. At depth, the real parts of the insulative and conductive kernels differ strongly, even in sign, and like the tipping angle, they become less oscillatory. Input parameters are described in the text.

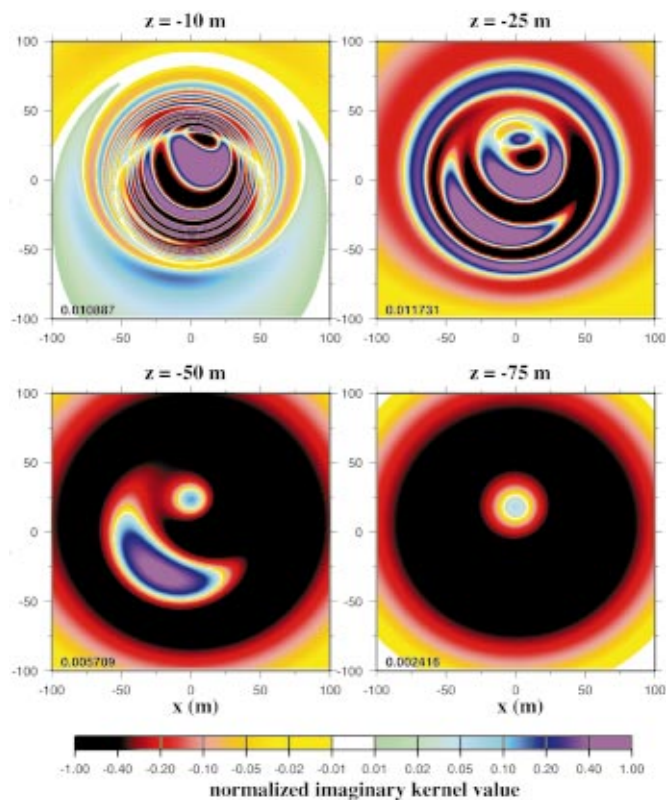


FIG. 9. (Color) Same as Fig. 8, but only the imaginary parts of the kernel, $K(q, \mathbf{x}_0; \mathbf{r})$, are shown at different depths for the conductor. Like the real part, the imaginary part of the conductive kernel becomes less oscillatory with depth. The imaginary part of the insulating kernel is identically zero.

that still maintains some physical relevance, we will now consider problems in which this three-dimensional (3D) structure is effectively reduced to one dimensional (1D). As discussed in Sec. IV B, if water density is translation invariant in the horizontal direction, that is if it is horizontally stratified, the forward problem for the NMR voltage response simplifies to a single depth integral. Under these circumstances, for coincident circular transmitter and receiver loops, Eq. (4.21) can be rewritten as

$$V(q) = \int dz \hat{K}(q, \mathbf{0}; z) \hat{n}_N(z), \quad (5.1)$$

where $\hat{K}(q, \mathbf{k}; z)$ was defined in (4.31), and where n_N is the position dependent number density of (detectable) nuclear magnetic moments, which is twice the molecular number density, n , for water. It is convenient to define the normalized density $n_v(z) = n_N(z)/2n_{\text{H}_2\text{O}}$ using bulk number density of water $n_{\text{H}_2\text{O}} = 3.35 \times 10^{22} \text{ cm}^{-3}$. Clearly $0 \leq n_v(z) \leq 1$, but in typical geophysical applications $n_v(z) \leq 0.25$. Equation (5.1) is then rewritten in the form

$$V(q) = \int dz \hat{K}_v(q; z) n_v(z), \quad (5.2)$$

with $\hat{K}_v(q; z) = 2n_{\text{H}_2\text{O}} \hat{K}(q, \mathbf{0}; z)$. Like the 3D kernel on which it is based, the 1D kernel, \hat{K}_v , is complex.

Figure 10 displays examples of the real and imaginary parts of $\hat{K}_v(q, z)$ for a variety of pulse moments, q , and conductivity structures ($\sigma = 0.1 - 0.001 \text{ s/m}$). The horizontal integral in Eq. (4.31) has been performed numerically at each depth over an area extending to four times the loop radius from the center of the loop in all directions ($-200 \text{ m} \leq x, y \leq 200 \text{ m}$). Several observations are worth noting. (1) Independent of q or σ , the real kernels are oscillatory near the surface, peak, and then decay at depth. The oscillations are not, in general, about zero. The peak amplitudes of the real kernels decrease as q and conductivity increase. (2) The extent of the oscillatory part and the depth of the peak in the real kernels depend on q . The real kernel penetrates deeper for large q . (3) Conductivity affects the deep parts of the real kernels more than the shallow parts. The nature of the oscillatory part of the real kernels is less strongly dependent on conductivity. In contrast, the depth and shape of the peak in the real kernels depend strongly on the conductivity structure of the subsurface, particularly at high q . (4) Like the real kernels, the imaginary kernels penetrate more deeply with q , but are not oscillatory near the surface. They strengthen with increased conductivity.

Several implications of the above observations are apparent. (1) Although the real kernels are oscillatory near the surface, they possess substantial sensitivity to near surface water because they do not oscillate about zero even at high q . (2) Sensitivity to water below the shallow subsurface is only contained in the high q real kernels and the imaginary kernels. (3) Subsurface conductivity structure affects the deep parts of the kernels more than the shallow parts. The net effect is that resolution near the surface, say in the top 20 m, is substantially better than at greater depths, in particular below about 50 m. Resolution at intermediate and greater

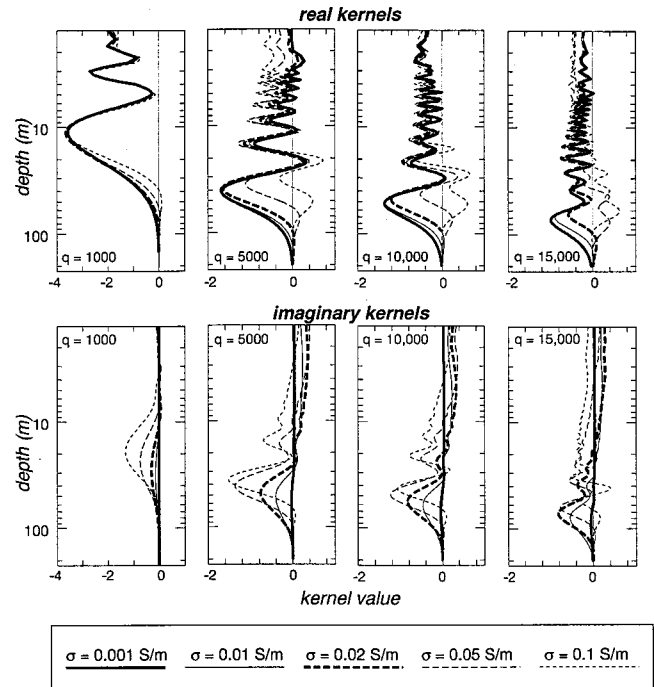


FIG. 10. Examples of the real (top row) and imaginary (bottom row) parts of the one-dimensional kernels, $\hat{K}_v(q, z)$, for a variety of conductivity structures ranging from an effective insulator ($\sigma = 10^{-3} \text{ s/m}$) to a fair conductor ($\sigma = 10^{-1} \text{ s/m}$) and a variety of pulse moments, q , ranging from $10^3 a$ ms to $1.5 \times 10^4 a$ ms. Different q values are arrayed columnwise and conductivities are specified by the various line types shown in the legend at the bottom of the figure. Kernels are in units of 10^2 nV/m .

depths is dependent on using high q real data and imaginary data. Discrepancies between the insulative and conductive kernels indicate that inferences using insulative kernels about water content and distribution below some conductivity-dependent cutoff depth, 20–30 m for $\sigma \sim 0.05 \text{ s/m}$, would be suspect.

C. The inverse problem for horizontally stratified water

Equation (5.2) is the basis for a linear inverse problem to estimate the distribution of horizontally stratified water in the subsurface. The noise characteristics of the data and *a priori* expectations about subsurface conductivity and water distribution should both inform the choice of inversion methodology and model parametrization. It is beyond the scope of this paper to characterize the inverse problem fully by performing a systematic study for a wide range of noise settings, conductivities, and water distributions with a set of different inversion methodologies. Rather, we will investigate here the characteristics of the inverse problem in the simplest of settings to highlight the nature of the inferential errors introduced by inaccurately modeling the effects of conductivity and to assess the utility of including the imaginary conductive kernels and data in the inversion.

At short times, directly after the transmitted signal, the attenuation of the received voltage response, $V(t)$, of an NMR experiment can be neglected and it may be written in the form,

$$\begin{aligned}
 V(t) &= \text{Re}(V_0 e^{-i(\omega_L t + \varphi)}) \\
 &= V_R \cos(\omega_L t + \varphi) + V_I \sin(\omega_L t + \varphi), \quad (5.3)
 \end{aligned}$$

where φ is the initial phase of the transmitted signal and V_R and V_I are the real and imaginary parts of the initial amplitude of the complex voltage V_0 . With a quadrature detection scheme, the rapid oscillations of the detected signal at the Larmor frequency are removed and what is measured are the real and imaginary parts of the complex envelope function. For very short times, the envelope function is nearly constant and given by $V(q)$ in (4.17), which is then precisely $V_0 = V_R + iV_I$. We call V_R and V_I the real and imaginary data. Together they define the phase of the envelope of the received signal: $\phi_V = \arctan(V_I/V_R)$ relative to the transmitted signal.

For simplicity, the problem is discretized by defining the water volume fraction, $n_v(z)$, as constant in each of L layers, $(z_0, z_1), (z_1, z_2), \dots, (z_{L-1}, z_L)$, with $z_0=0$ being the surface. The discrete model parameters n_j^v are, therefore, defined via $n_v(z) = n_j^v$, for $z_{j-1} \leq z < z_j$ ($j=1, \dots, L$). A discrete set of pulse parameters, q , are employed in any real NMR survey: $q_i, (i=1, \dots, N)$. The forward problem, Eq. (5.2), may then be written in the discrete form,

$$d_i \equiv V_0(q_i) = \sum_{j=1}^L \hat{K}_{ij} n_j^v, \quad (5.4)$$

in which

$$\hat{K}_{ij} \equiv \int_{z_{j-1}}^{z_j} dz \hat{K}_v(q_i). \quad (5.5)$$

In matrix notation, (5.4) is re-expressed simply as

$$\mathbf{d} = \hat{\mathbf{K}} \mathbf{n}^v, \quad (5.6)$$

where, to recapitulate, the data vector \mathbf{d} has N complex elements, the model vector \mathbf{n}^v has L real elements, and the complex inversion matrix $\hat{\mathbf{K}}$ is $N \times L$. Since the model vector \mathbf{n}^v is real, for computational purposes one may separate the real and imaginary parts of \mathbf{d} and $\hat{\mathbf{K}}$ so that the data vector is considered to have $2N$ real elements and the inversion matrix is also real and of size $2N \times L$. Thus, although the data and kernels are complex in a conductive medium, the separation of the real and imaginary parts allows one to manipulate the data vector and the inversion matrix in such a way as to treat them as real variables.

Figure 11 displays noise-free synthetic data for three models, each consisting of a single layer of water at different depths: 10–20 m, 30–45 m, and 60–80 m. Within each layer, water saturation is taken to be constant and complete, $n_v = 1$. Because the problem is linear, water volume fractions less than unity would simply linearly rescale all results shown here. Both real and imaginary data, V_R and V_I , are shown for q values ranging from 100 to 1.5×10^4 A-ms for a conductor ($\sigma = 0.05$ S/m) and for an effective insulator ($\sigma = 0.001$ S/m). The nineteen q values shown in Fig. 11 and used in the inversions below are 100, 250, 500, 750, and 1000 to 15 000 in increments of 1000. In every case, the data curves are very simple: they approach zero at low q , peak at

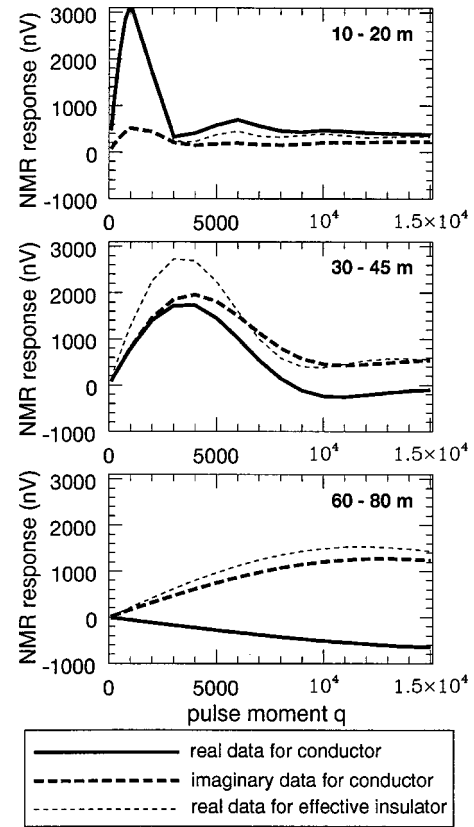


FIG. 11. Noise-free synthetic data (V_R, V_I), for three models consisting of a single water layer at different indicated depths, plotted vs pulse moment, q , ranging from 100 A-ms to 15 000 A-ms. The legend describes the meaning of the curves where $\sigma = 0.05$ S/m for the conductor and $\sigma = 0.001$ S/m for the effective insulator. Units are nV, and it should be recalled that $V_I = 0$ for an insulator.

some intermediate value of q , depending on the depth of the water layer, and then decay to zero. The simplicity of the curve structures means that a fine sampling is not necessary to capture the information in the data (a fact exploited in [5]), but also means that the information content of the data is not particularly high. For shallow water layers, the imaginary data are nearly zero and the conductive and insulative real data are nearly identical. For water at greater depths, however, the conductive and insulative real data diverge from one another and the magnitude of the imaginary conductive data grows to eventually overtake that of conductive real data. For water at great depth, the real data computed for an insulating subsurface may actually differ in sign from the real data computed for a conducting subsurface.

Equation (5.6) is inverted by using the singular value decomposition (SVD) [26] of the inversion matrix

$$\hat{\mathbf{K}} = \mathbf{U} \mathbf{\Lambda} \mathbf{V}^T, \quad (5.7)$$

where \mathbf{U} and \mathbf{V} are the left and right eigenvector matrices of the nonsquare matrix $\hat{\mathbf{K}}$, and $\mathbf{\Lambda}$ is the diagonal matrix of singular values λ_i ($i, j = 1, \dots, L$). There are certainly better inversion methods for NMR data in which a wide variety of regularization schemes could be applied, but we choose the SVD for simplicity of presentation here. Other inversion schemes and model parametrizations will be explored in future work [19].

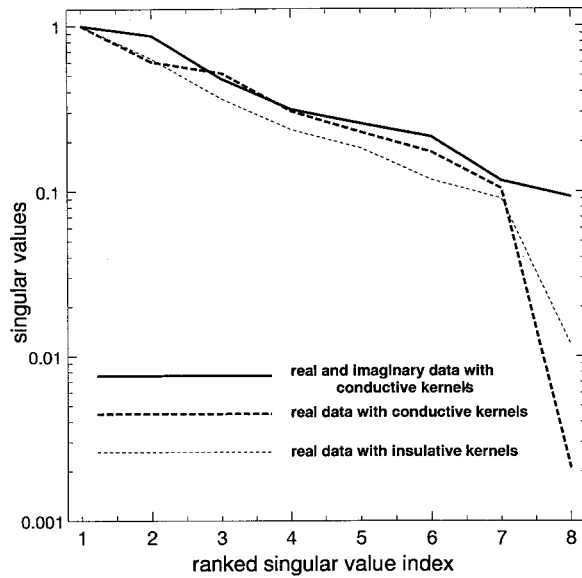


FIG. 12. Normalized singular values (λ/λ_{\max}) of the NMR inversion matrix, $\hat{\mathbf{K}}$, for inversions using three different types of data with integral kernels constructed for different conductivity structures: (thin dotted line) real voltage response with insulative kernels, (thick dashed line) real voltage response with conductive kernels ($\sigma=0.05$ S/m), and (solid line) real and imaginary voltage response for the same conductive kernels. It is evident that the use of both real and imaginary voltage response data greatly improves the stability of the inversion matrix.

The model is defined on eight discrete layers bounded by the following depths: $z_1=5$ m, $z_2=10$ m, $z_3=20$ m, $z_4=30$ m, $z_5=45$ m, $z_6=60$ m, $z_7=80$ m, $z_8=100$ m. Layer thicknesses increase with depth due to reduced intrinsic resolution with depth (a formal maximal inner product procedure was used in [5] to obtain a similar sequence of depths). With this parametrization, there are eight model parameters and 19 real data and 19 imaginary data (if the latter are used). Thus, there are eight singular values of the (19×8 or 38×8) inversion matrix $\hat{\mathbf{K}}$.

The stability of a matrix can be quantified by the range of singular values. A useful condition number is the ratio of the minimum to maximum singular values: $\text{cond}(\hat{\mathbf{K}}) = \lambda_{\min}/\lambda_{\max}$. Figure 12 displays normalized singular values (λ/λ_{\max}) for three different inversion matrices: (1) real data (V_R) with real insulative kernels in $\hat{\mathbf{K}}$, (2) real data (V_R) with real conductive kernels ($\sigma=0.05$ S/m) in $\hat{\mathbf{K}}$, and (3) real and imaginary data (V_R, V_I) for the real and imaginary conductive kernels in $\hat{\mathbf{K}}$. Larger condition numbers (closer to unity) indicate more stable matrices. As Fig. 12 shows, the use of imaginary data improves the stability of $\hat{\mathbf{K}}$ appreciably. More stable matrices yield relatively small noise magnification upon inversion because, for example, if the noise level is normally distributed and uncorrelated with constant rms noise level ϵ , then the model covariance matrix is $\mathbf{C}_m = \epsilon^2 \mathbf{V} \mathbf{\Lambda}^{-2} \mathbf{V}^T$. Thus, very small singular values magnify the effect of noise on the estimated model. This motivates the ranking and winnowing or weighting of the singular values to damp or regularize the inversion. If \mathbf{W} is a diagonal weighting matrix, then, the estimated model will be given by

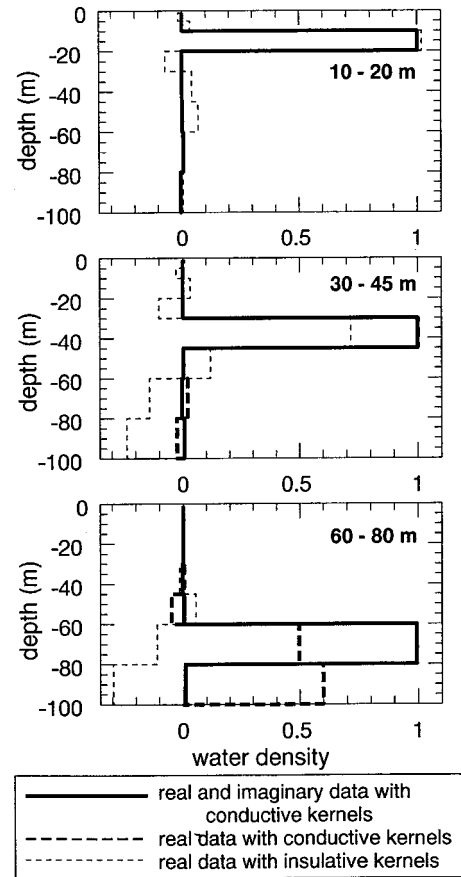


FIG. 13. Results for three synthetic inversions in which noise-free synthetic data computed for a conductive ($\sigma=0.05$ S/m) subsurface are inverted for three different single-layer models: constant and complete saturation at 10–20 m, 30–45 m, and 60–80 m. Each model is inverted in three ways: (1) real data (V_R) are inverted with real insulative kernels, (2) real data are inverted with real conductive ($\sigma=0.05$ S/m) kernels, and (3) real and imaginary (V_I) data are inverted with real and imaginary conductive kernels. The legend relates the line types with the type of inversion. Inversions are subjected to inverse singular value weighting described in the text.

$$\mathbf{n}^v = \mathbf{V}(\mathbf{W}\mathbf{\Lambda}^{-1})\mathbf{U}^T \mathbf{d}. \quad (5.8)$$

The choice of \mathbf{W} depends on the signal-to-noise (SNR) characteristics of the data set. For NMR surveys with SNR ranging from 10 to 100, singular values below about $\lambda_{\max}/10$ should be down weighted or discarded altogether. In the synthetic results shown here we apply a cosine-shaped weight to the inverse singular values with a value of 1.0 for $\lambda \geq \lambda_{\max}/10$ and 0.0 for $\lambda \leq \lambda_{\max}/100$. This damping is appropriate for fairly high SNR NMR surveys. To simulate noisier surveys, more severe damping would be necessary.

Figure 13 presents the results of synthetic inversions for three different models of water distribution. In each of the three models, there is complete saturation ($n_v=1$) in a single horizontal layer (10–20 m, 30–45 m, or 60–80 m) and the remaining layers are dry ($n_v=0$). For each of the input models, noise-free synthetic real (V_R) and imaginary (V_I) data are computed with the conductive kernels ($\sigma=0.05$ S/m) and then inverted in three different ways: (i) real data with real insulative (i.e., adiabatic—see Sec. II C) kernels, (ii) real data with real conductive kernels, (iii) and real and imagi-

nary data with real and imaginary conductive kernels. Inversion (i) then uses an incorrect kernel, similar to those used in the previous literature [4–6], and will allow us to estimate the resulting errors in the inferred water distribution. Optimally, we would like to use real experimental data here, but as discussed earlier, this is currently unavailable. The conclusions from this analysis are as follows. (1) Near surface water (e.g., 10–20 m) can be fairly accurately inferred using real data alone. Imaginary data provide little improvement and the degrading effect of the use of (incorrect) insulative kernels is relatively small. (2) For water at intermediate depths (e.g., 30–45 m), the estimated model begins to diverge significantly from the input model if insulative kernels are used. We expect that similar errors are present in reported inversions of experimental data [4,6] in this depth range. The use of real data alone with conductive kernels, however, remains faithful to the input model. (3) For deep water (60–80 m), the use of insulative kernels is disastrous. The anticorrelation at depth between the real insulative and conductive kernels in Fig. 10 imparts an unphysical *negative* value to the estimated water density if the insulative kernels are used in the inversion. Positivity constraints on the water profile could be applied to overcome this problem, but in any event the inferred water distribution would be erroneous, and previously reported experimental inversions in this depth range certainly cannot be trusted. The nature of the induced errors is a function of *ad hoc* choices of model parametrization, damping, etc. Finally, there is a significant improvement in resolution if imaginary data are used, relative to inversions that employ only real data, with the conductive kernels.

The synthetic inversions shown here ignore many of the practical and theoretical issues that must be confronted in an inversion of data from real NMR surveys. The implications

for NMR surveys are clear, however. The ability to estimate the density and distribution of water in the deep subsurface depends critically on the use of the generalized theory to accurately model the effects of finite conductivity in the propagating medium. The use of imaginary data stabilizes the inversion and provides useful additional information, which improves resolution, particularly for deep water. These implications would be particularly true for stronger conductors, commonly encountered with alkaline entrained waters, than we have considered here.

In future work, improved inversion methodologies will be investigated in a variety of SNR regimes for models that include the effects of vertical variations in conductivity. For a multilayered conductivity structure, the inverse problem becomes effectively nonlinear because the conductivity of the propagating medium is a function of the unknown water volume fraction (as well as of the chemical composition of the water and the porosity of the subsurface). Improved methodologies will include different model parametrizations and regularization schemes, such as the application of *a priori* constraints (such as hard bounds on water volume fraction), more careful characterization of covariances in the model coefficients, and the use of different transmitter and receiver geometries. Variations in loop geometries, in particular, away from coincident circles can be used to improve SNR and to provide more and different kinds of data that may further stabilize the inversion.

ACKNOWLEDGMENTS

The support of the DOE through Contract No. DE-FG07-96ER14732 is gratefully acknowledged. We are indebted to M. Blohm, P. Hoekstra, A. Legchenko, P. Valla, and E. Fukushima for numerous conversations regarding geophysical field measurements and instrumentation.

-
- [1] See, e.g., A. Abragam, *Principles of Nuclear Magnetism* (Oxford University Press, New York, 1983).
- [2] In medical applications the surface NMR technique discussed here is known as “rotating frame imaging” or “nutration imaging” using a surface pickup coil [see, e.g., D. I. Hoult, J. Magn. Reson. **33**, 183 (1978)]. The technique still requires a laboratory generated static field.
- [3] Invasive borehole NMR tools have been in use in the oil industry for some time. See, e.g., R. L. Kleinberg, *The Industrial Physicist* **2** (2), 18 (1996). However, due either to geometric limitations of the transmitter loop or to the fact that the tool generates its own static field, it is sensitive to oil or water only to within a fraction of a meter of the borehole into which it is lowered.
- [4] See, e.g., D. V. Trushkin, O. A. Shushakov, and A. V. Legchenko, *Geophys. Prospect.* **43**, 623 (1995).
- [5] A. V. Legchenko and O. A. Shushakov, *Geophys. J.* **63**, 75 (1998).
- [6] M. Goldman, B. Rabinovich, M. Rabinovich, D. Gilad, I. Gev, and M. Schirov, *J. Appl. Geophys.* **31**, 27 (1994).
- [7] A preliminary version of our results has appeared in P. B. Weichman, E. M. Lavelly, and M. H. Ritzwoller, *Phys. Rev. Lett.* **82**, 4102 (1999), and has also been featured on the Physical Review Focus website, *Dowsing with Nuclear Magnetic Resonance*, <http://focus.aps.org/v3/st27.html>, May 17, 1999.
- [8] Finite skin depth effects, computable as special cases of the general theory we present, have been considered previously in terms of dissipation and resulting NMR voltage phase shifts in solid state [see, e.g., M. D. Harpen, *Phys. Med. Biol.* **33**, 597 (1988)] and biological systems [see, e.g., P. A. Bottomely and E. R. Andrew, *ibid.* **23**, 630 (1978)].
- [9] See, e.g., K. R. Foster, H. P. Schwan, and M. A. Stuchly, *Crit. Rev. Biomed. Eng.* **17**, 25 (1989).
- [10] P.-M. L. Robitaille, A. Kangarlu, and A. M. Abduljalil, *J. Comput. Assist. Tomogr.* **23**, 845 (1999).
- [11] A. M. Abduljalil and P.-M. L. Robitaille, *J. Comput. Assist. Tomogr.* **23**, 832 (1999).
- [12] A. Kangarlu, B. A. Baertlein, R. Lee, T. Ibrahim, L. Yang, A. M. Abduljalil, and P.-M. L. Robitaille, *J. Comput. Assist. Tomogr.* **23**, 821 (1999).
- [13] See, e.g., J. M. Jin, J. Chen, W. C. Chew, H. Gan, R. L. Magin, and P. J. Dimbylow, *Phys. Med. Biol.* **41**, 2719 (1996).
- [14] J. D. Jackson, *Classical Electrodynamics*, 2nd ed. (Wiley, New York, 1975).
- [15] Theories and experiments on the physical origin and magnitudes of the two time constants T_1 and T_2 for fluids in geo-

- physical porous materials are discussed in R. L. Kleinberg, W. E. Kenyon, and P. P. Mitra, *J. Magn. Reson. A* **108**, 206 (1994), and references therein.
- [16] This is especially the case when the transmitter loop is also used as the receiver loop. The NMR signal induced in the transmitter loop can then only be measured after shut off of the transmitter source current.
- [17] See, e.g., Goldman *et al.*, *J. Appl. Geophys.*, Ref. [6], and D. V. Trushkin *et al.*, *Geophys. Prospect.*, Ref. [4]. The latter authors consider the effects of a finite conductivity on the NMR response, concluding that it yields a significant effect, by simply substituting a nonadiabatic computation of \mathbf{B}_T into (2.28) in place of \mathbf{B}_0 (appropriate to the case of coincident transmitter and receiver coils). Since they are considering high conductivity soils with skin depth on the order of 10 m and modeling water content down to nearly 100 m, conductivity effects are clearly dominant. Although the formula they use then contains the correct dynamics (2.2), of the nuclear spins, it misses the equally important memory effect, and the imaginary part of the response contained in (2.21).
- [18] Inclusion of a finite ϵ' would cure the apparently unphysical instantaneous arrival of the exponential tail of the diffusing front at the point \mathbf{r} . The leading edge would then only arrive after a delay time $r/\epsilon'c$ much shorter than the time scales of interest in this work.
- [19] D. R. Lun, P. B. Weichman, M. H. Ritzwoller, and E. M. Lavelly (unpublished).
- [20] See, e.g., A. A. Kaufman, *Geophysical Field Theory and Method* (Academic Press, New York, 1992), Part A, p. 412.
- [21] D. I. Hoult and R. E. Richards, *J. Magn. Reson.* **24**, 71 (1976).
- [22] See, e.g., J. M. Hendrickx, T. Yao, A. Kearns, P. Hoekstra, R. J. Blohm, M. W. Blohm, P. B. Weichman and E. M. Lavelly, DOE Report No. DE-FG07-96ER14732, 1999 (unpublished).
- [23] Strictly speaking, if one maintains the convention $-\pi/2 < \zeta \leq \pi/2$, (4.11) is not always valid. If it requires the addition or subtraction of an odd multiple π to bring ζ , as defined by this equation, back into this interval [as, for example, if $3\pi/2 \geq r/\delta_s(\omega_L) \geq \pi/2$], one must then instead choose $\hat{\mathbf{b}}(\mathbf{r}, \omega_L) = \hat{\rho}$. A perhaps better convention for the purposes of the EM problem is to demand only that $\zeta(\mathbf{r}, \omega_L) \rightarrow 0$ for $r/\delta_s(\omega_L) \rightarrow 0$, and that $\hat{\mathbf{b}}(\mathbf{r}, \omega_L)$ and $\zeta(\mathbf{r}, \omega_L)$ be defined continuously for all other positions and frequencies. This has the disadvantage of requiring global, rather than just local, knowledge of the phase, but succeeds in removing artifactual discontinuous changes in the phase and the polarization vector.
- [24] The quadrature component of the NMR voltage is indeed measured, though with poor accuracy, by the instruments currently in use for ground-water imaging, and is found to vary substantially from site to site (Mark W. Blohm, private communication). However, prior to the present work, there has been no attempt to analyze this part of the signal either to correlate it with ground conductivity or for imaging purposes.
- [25] See, e.g., W. E. Kenyon, P. I. Day, C. Straley, and J. F. Willemsen, SPE Report No. 2529, SPE Annual Technical Conference, 1986 (unpublished). A standard laboratory technique for measuring T_1 involves the application of a 180° , pause, 90° pulse sequence. However this requires a uniform tipping field, which is unavailable in both geophysical borehole and geophysical surface NMR contexts.
- [26] See, e.g., R. L. Parker, *Geophysical Inverse Theory* (Princeton University Press, Princeton, NJ, 1994).